Project information

Project full title	EuroSea: Improving and Integrating European Ocean Observing and Forecasting Systems for Sustainable use of the Oceans
Project acronym	EuroSea
Grant agreement number	862626
Project start date and duration	1 November 2019, 50 months
Project website	https://www.eurosea.eu

Deliverable information

Deliverable number	D7.1
Deliverable title	**Report on demo mission and dissemination pathways of obtained data based on different observational platforms**
Description	This document describes the deployment of instrumentation in the Eastern tropical Atlantic area and shows the preliminary data acquired.
Work Package number	7
Work Package title	Ocean climate indicators demonstrator
Lead beneficiary	GEOMAR
Lead authors	Björn Fiedler (GEOMAR)
Contributors	Romain Cancouët (Euro-Argo ERIC), Hervé Claustre (SU/LOV), Laurent Coppola (SU/LOV), Leticia Cotrim da Cunha (UERJ), Marine Fourrier (SU/LOV), Fabrice Hernandez (IRD/LEGOS/UFPE/DOCEAN/LOFEC), Melf Paulsen (GEOMAR), Cathy Wimart-Rousseau (GEOMAR)
Due date	31.08.2022
Submission date	28.10.2022
Comments	This deliverable is delayed by 2 months. Retrieving the saildrone and hence the onboard data took much longer than anticipated. The drone got only recovered in July. Due to the delayed data delivery to GEOMAR, the work on the data was also delayed. Furthermore, the team had to wait for the post-calibration of the CO_2 sensor of the saildrone, which was carried out by the collaborating National Oceanic and Atmospheric Administration (NOAA) in the US.

https://doi.org/10.3289/eurosea_d7.1

Table of contents

Executive summary

This report presents the first results of work package 7 (Task 7.3) on "Report on demo mission and dissemination pathways of obtained data based on different observational platforms".

In order to improve our understanding of the ocean's role in the Earth's climate change, and to assess long-term changes in the oceanic carbon cycle, sustained high-quality *in situ* measurements are needed. Due to its peculiar geographical position, the Eastern Tropical Atlantic Ocean is impacted by multiple coupled climate changes, varying over numerous timescales, and impacting surrounding areas (Foltz et al., 2019). Thus, changes occurring in this region impact the global ocean as it is connected to the Southern and Northern branches of the Atlantic meridional overturning circulation. Task 7.3 aims to develop indicators for carbon flux observations in this region based on the improvement of existing components and on the deployment of new observing tools.

Thus, this task considers the use of biogeochemical (BGC) Argo floats, moored buoys, and autonomous surface vehicles such as Wave Glider and Saildrone for the acquisition of high-quality carbon measurements at a regional scale. A pilot mission has been designed and embedded into existing components of the Tropical Atlantic Observing System (TAOS) to improve the spatio-temporal coverage of carbon measurements in this area. This approach aims to circumvent observational gaps and disparities observed in response to conventional data collections that undersample some biogeochemical provinces. By providing high-quality carbon measurements, this task aims to enhance the robustness of tropical carbon flux estimates and, thus, our understanding of the oceanic response to anthropogenic carbon invasion.

This report, resulting from the contribution of numerous laboratories (GEOMAR, SU/LOV, Euro-Argo ERIC, UERJ, IRD/LEGOS/UFPE/DOCEAN/LOFEC), summarises the multi-platform deployment approach followed in this region and presents the main characteristics of the implemented tools. In addition, the first outcomes and results obtained by the autonomous platforms are presented. Finally, the first conclusions of this multi-platform approach are synthesised.

Disclaimer: This document represents the situation at the time of data evaluation and writing of the report which is primarily based on data from 2021/2022 or not fully processed data. As BGC-Argo floats and Autonomous Surface Vehicles (ASVs) are still in operation or have to be reprocessed, more data is coming in and the database is growing daily. This will allow us to improve the statistics of our analysis and hence the robustness of the results. Therefore, the results presented here are based on the *status quo* and are not necessarily the final word on these matters. We therefore point out that further analyses will and need to be carried out.

1. Introduction

1.1. The Tropical Atlantic area

The Tropical Atlantic basin, covering both sides of the Atlantic Ocean, is home to multiple coupled oceanic and climate variations occurring on decadal and interannual timescales. Extending from Southern Florida to the Gulf of Mexico, and through the Caribbean to the Angola coast, the Tropical Atlantic faces several natural and anthropogenic-related fluctuations due to its equatorial position and its coastal boundaries. Firstly, this area is influenced by both El Niño (Chang et al., 2006) and the North Atlantic atmospheric oscillations (NAO; Czaja et al., 2002). Also, the tropical Atlantic variability is due to numerous subtropical cells and cyclones that could form storms, rainfall, and flooding.

From an oceanic point of view, due to its connection with subtropical and higher latitude regions, the Tropical Atlantic area is impacted by the Atlantic Meridional Overturning Circulation (AMOC; Boers, 2021), the Atlantic Multi-Decadal Oscillation (AMO), and gyres. In consequence, the biogeochemistry of this region presents large variability, with anoxic conditions regularly observed along some shelves (Brüchert et al., 2006; Machu et al., 2019), high productivity areas, local oxygen depletion associated with intense respiration and remineralization due to important organic matter inputs close to coastal areas (Chen and Borgers, 2009), or freshwater discharges and nutrients inputs from the three large rivers. Moreover, Oxygen Minimum Zones (OMZ) are found at intermediate depths in the Eastern Tropical Ocean (Karstensen et al., 2008). These depleted oxygen zones are the seat of CO_2 releases, and other greenhouse gases like N_2O. Also, it has been recently stated that the Tropical Atlantic is the second largest source of CO_2 for the atmosphere (after the Tropical Pacific), releasing about 0.10 Pg C y^{-1} (Landschützer et al., 2014), over a long time period, with unavoidable consequences for marine organisms and ocean acidification. In addition, attention must be paid to eddies that are generated in the eastern side of the basin connecting the eastern boundary upwelling systems with the open oceans, transporting oxygen-poor and nutrient-rich waters into the oligotrophic ocean and impacting the mean state (Schütte et al., 2016a, b).

All of the aforementioned climate variations occur in a changing climate. For example, increasing trends in sea surface temperature, salinity, upper-ocean heat content, and rainfall have emerged in the past decade (Tokinaga and Xie, 2011; Durack et al., 2012; Servain et al., 2014). At the same time, acidification has been examined in this region (Lefèvre et al., 2016). Thus, in addition to numerical models, it is urgent to acquire *in situ* data in this region to predict how these changes are and will affect in the near future the biogeochemistry of this area and its role as a sink or source of atmospheric CO_2. Indeed, it appears essential to understand and monitor changes in the tropical Atlantic region in order to better understand the climate change impact on this area, validate and improve models, and address many societal challenges.

1.2. Chemistry of Carbon Dioxide in Seawater

Carbon is stored in three main reservoirs linked together by exchange fluxes, and it moves between these reservoirs through a variety of processes. The oceanic carbon cycle is a central process of the global carbon cycle, containing both organic and inorganic carbon. In the ocean, the dissolution of carbon dioxide (CO_2), which reacts with water, follows a series of chemical equilibria. These reactions, governed and connected by equilibrium reactions, give rise to four different chemical species that form the oceanic carbonate system: CO_2 in aquatic solution, carbonic acid, bicarbonate, and carbonate (*i.e.*, CO_2 (aq), H_2CO_3, HCO_3^-, CO_3^{2-}). Nevertheless, individual species of the carbonate system cannot be measured directly. To overcome this

issue, four parameters that can be measured at high accuracy have been developed to completely describe (with ancillary information) the CO_2 system in seawater (Dickson et al., 2007).

These four parameters are:

- Total alkalinity (TA)
- Fugacity/partial pressure of CO_2 in gas phase in chemical equilibrium with seawater (fCO$_2$/pCO$_2$)
- Total hydrogen ion concentration (pH)
- Total dissolved inorganic carbon (DIC)

Theoretically, because of the relative consistency of the chemical constituents of seawater, a complete description of the marine CO_2 system can be obtained based on only two of the four measurable carbon parameters, together with the equilibrium constants, temperature, pressure, and salinity (Dickson et al., 2007).

1.3. Marine Carbon Dioxide System Observations

To assess long-term changes in ocean chemistry, accurate and sustained time-series datasets are needed to decipher long-term trends to seasonal changes and to better constrain and predict future changes. Over the last few decades, numerous oceanographic cruises (*e.g.* PIRATA, GO-SHIP, etc.; Foltz et al. 2019) or fixed station measurements (buoys, moorings) have been implemented in the Tropical Atlantic area. However, these cruises do not cover full temporal (seasonal) cycles leading to biased observations. Indeed, in response to biological, physical, and chemical processes, in addition to anthropogenic modifications, the dynamic marine CO_2 system changes on daily to centennial timescales, with seasonal, interannual, and decadal variabilities. Therefore, ship-based observing strategies that are oriented to particular months and regions, including some locations where current sampling methods are not feasible (*e.g*., ocean areas with sea ice), cannot adequately capture the spatiotemporal dynamic variability of the carbonate system parameter.

In consequence, datasets based on these historical sampling strategies have "observational gaps" (Tanhua et al., 2019) that need to be filled. To circumvent these gaps and overcome the remoteness of numerous under sampled areas, autonomous platforms such as moorings, profiling floats, underwater gliders, or emerging autonomous surface vehicles have been deployed at global scale, mainly thanks to the development of miniaturised autonomous sensors. In comparison to ship-based measurements, these platforms have numerous advantages: the overall low cost of deployment, platforms remaining in an area of interest for a long time, and being non-impacted by weather conditions, minimal human resources needed, and measurements closer to the ocean surface.

Recently, pH and pCO$_2$ sensors suitable for deployment on autonomous surface vehicles have been developed (Sabine et al., 2020). On Argo floats, two pH sensors using the same technology are implemented: the Deep Sea DURAFET and the SBE Float Deep SeaFET. Both sensors are typically installed on the head of the float and rely on the same technique: an ISFET (Ion Sensitive Field Effect Transistor) coupled with a reference electrode composed of an AgCl pellet. The pH is derived proportionally from the voltage between the ISFET and the reference electrode (Bittig et al., 2019). The accuracy ranges from ±0.05 as stated by the manufacturer to ±0.005 after data is adjusted (Johnson et al., 2017).

While numerous pCO$_2$ sensors using a range of sensing techniques are available from multiple vendors (Martz et al., 2015), pCO$_2$ data presented hereafter have been obtained by two systems that sequentially measure atmospheric and seawater pCO$_2$ using a nondispersive infrared detector. In these systems, a LICOR

determines the CO_2 gas concentration by measuring the absorption of infrared energy as a sample gas flows through an optical path. Nevertheless, as slight differences can be observed between the ASVCO2 system installed in the Saildrone platform and the one implemented in the Wave Glider (a VeGAS CO_2 system), a detailed description of these two setups can be found in section 2.2.

2. Strategic Approach and Assets

2.1. Background

The tropical Atlantic area, due to its geographical position, is impacted by multiple physical and biogeochemical processes that, in turn, have relevant impacts on both the global overturning circulation and the surrounding coastal areas and their population. In order to better understand and constrain the phenomena occurring in this region, *in situ* observing systems have been developed in this area and many observational networks are present (Figure 1), built on the backbone of the Prediction and Research Moored Array in the Tropical Atlantic (PIRATA; Bourlès et al., 2019) program initiated in 1997. A detailed description of the existing Tropical Atlantic observing system developed can be found in Foltz et al. (2019).
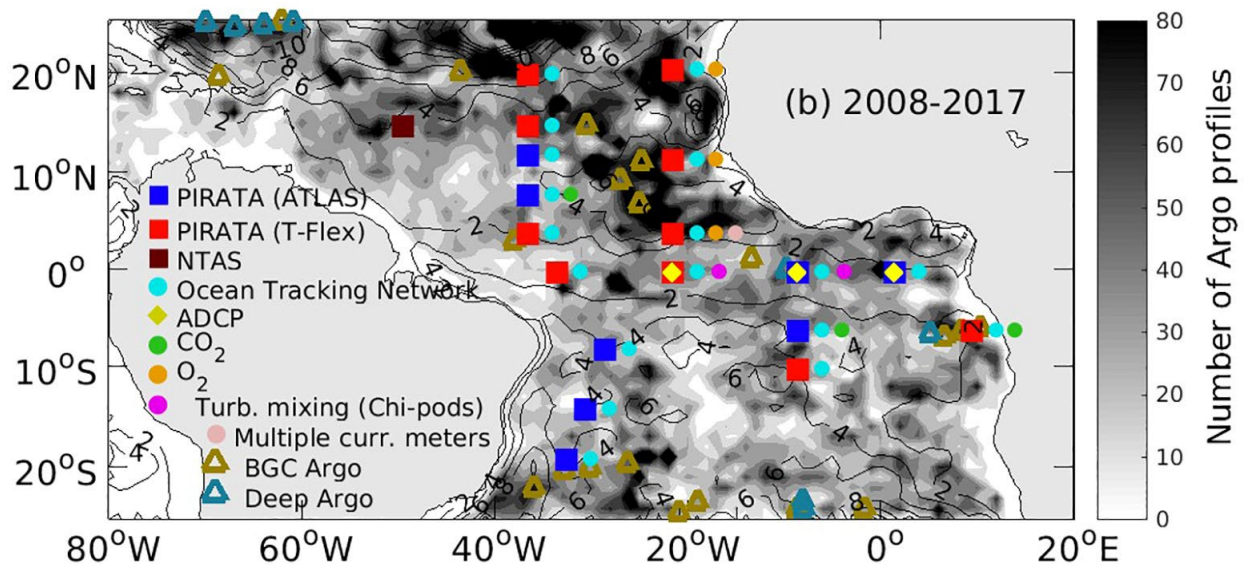

Figure 1. Map of the existing tropical Atlantic observing system (2008-2017) from Foltz et al., 2019.

Over the studied area, 18 moorings have been deployed and measure, near the surface and vertically, biogeochemical, and physical parameters (temperature, salinity, relative humidity, wind velocity, rainfall, and radiation). Several moorings can also measure ocean currents, turbulence, dissolved oxygen, or acoustics. In 2006 and 2008, CARIOCA (Carbon Interface Ocean Atmosphere) CO_2 sensors (NKE instrumentations), recording seawater fugacity ($fCO_2{}^{SW}$), sea surface temperature (SST) and dissolved oxygen (O_2) hourly in the surface ocean have been integrated on the 6°S, 10°W (Parard et al., 2010) and 8°N, 38°W PIRATA moorings that are maintained by French and Brazilian institutes, respectively. In 2017 and 2020, new CARIOCA sensors were installed at 6°S, 8°E and 0°N, 10°W. Moreover, other moorings and buoys, not maintained and operated in the frame of the PIRATA program, are present in the tropical Atlantic area: the Cape Verde Ocean Observatory (CVOO - 17.6°N, 24.3°W), the Northwest Tropical Atlantic Station for air-sea flux measurements (NTAS - 15°N, 51°W), the Melax air-sea buoy in the Senegalese part of the Canary current upwelling system

(14°N, 17°W) and numerous meteorological stations (*e.g.* the Cape Verde Atmospheric Observatory station (CVAO - 16°51'49"N, 24°52'02"W)).

Annual oceanographic PIRATA cruises are conducted and performed to ensure the maintenance of the PIRATA mooring network but also to perform conductivity-temperature-depth (CTD) casts and *in situ* biogeochemical parameters measurements. Thanks to these repeated transects, multi-annual changes can be studied. Deployments of autonomous platforms such as BGC-Argo floats or surface drifters can also occur. The Tropical Atlantic area is part of the GO-SHIP (Global Ocean Ship-based Hydrographic Investigations Program) program (Sloyan et al., 2019) which aims to conduct repeated high-quality hydrographic surveys with high spatial and vertical resolutions of physical, chemical, and biological parameters. Finally, monitoring changes and variability in this area is also done based on data acquired in the frame of the SOOP (Ship Of Opportunity Program; Goni et al., 2010) program that records data from volunteer merchant ships regularly crossing the area. Parts of the Atlantic SOOP network are operated in the European Research Infrastructure 'Integrated Carbon Observation System' (ICOS) and the 'Surface Ocean CO2 Reference Observing Network' (SOCONET). This network can be used as a potential reference for quality control of autonomous platform datasets as the standard-SOOP framework features, at least, routine pCO$_2$/fCO$_2$ observations. Nonetheless, it should be noted that this report will focus on the first results obtained and acquired by tools and platforms deployed in the frame of the EuroSea project. In consequence, in situ data acquired following classical sampling strategies (including SOOP-lines) will not be in the remaining of this report but will be taken up in the D7.6 report.

In order to improve our understanding of this area's physical and biogeochemical variabilities, and also to circumvent the low spatial and temporal resolutions associated with the classical observational tools, uncrewed autonomous platforms such as profiling Argo floats, underwater gliders, or surface vehicles have been deployed at a global scale (*e.g.,* Whitt et al., 2020), contributing to the densification of global databases. In the global ocean, biogeochemical parameters profiles are currently made by 442 active floats, of which 19 are in the tropical Atlantic area as defined in Figure 1[1]. These platforms may carry sensors measuring dissolved oxygen, chlorophyll-a, pH, and nitrate, allowing us to improve our knowledge, among others, of the ocean's carbon cycle and evolution, particularly ocean acidification. Additionally, autonomous platforms such as Wave Gliders (Manley and Willcox, 2010), a combination of sea-surface and underwater vehicle composed of a submerged glider that is attached to a surface float, have often been deployed in the tropical Atlantic within distinct programs. For example, since 2015, 4 Wave Gliders have been deployed near the Cape Verde archipelago and collected data on the exchange of CO$_2$, O$_2$ and N$_2$ between the ocean and the atmosphere. Finally, satellite-based observations can also be cited as another way to acquire (near) real-time data as sea surface temperature, salinity, height, solar radiations, rainfall, or surface chlorophyll-a.

Nonetheless, and even if a high degree of integration among the various observing components can be observed in the tropical area, accurately determining oceanic changes in response to anthropogenic impacts rely on sustained datasets both in time and space. Indeed, *in situ* data obtained during oceanographic cruises, while being reference data, cover limited spatiotemporal ranges. Conversely, satellite datasets give global coverage but only at the surface. Argo floats provide greater spatial and temporal variabilities than fixed stations and moorings but are dependent on oceanic circulation and subject to important post-deployment calibration processes. Thus, while having numerous strengths, all these data collection platforms, with

---

[1] https://www.ocean-ops.org/board?t=argo, Last accessed October 18th, 2022

regional disparities and low temporal resolutions, lead to "observational gaps" with an under-sampling of biogeochemical variables.

In order to fill these "observational gaps", the aim of task 7.3 was to upgrade existing components of the Tropical Atlantic Observing System for autonomous carbon observations (with the deployment of new CO_2 sensors on existing moorings, for example), whilst deploying news tools (BGC-Argo floats, Wave Gliders, Saildrone) equipped with instrumentation for high-quality carbon measurements.

2.2. Deployed Platforms

Saildrone

Saildrones (SD) are autonomous uncrewed surface ocean vehicles (USVs) equipped with a rigid sail and propelled by the wind. Sensors deployed on the Saildrone are powered by solar radiation and wave energy (Meinig et al., 2019). Such autonomous surface vehicle has been deployed in numerous oceanic regions (*e.g.,* Sabine et al., 2020). A Saildrone platform equipped with an ASVCO2 system (PMEL, NOAA) was deployed from Newport, RI (USA) in July 2021. After sailing 3,235nm over 75 days to reach the EuroSea mission operating area (Figure 2), the SD 1079 started recovering data on September 18th, 2021. The mission in the EuroSea area lasted 138 days and ended on February 3rd, 2022. SD 1079 was recovered safely in Jacksonville, FL (USA) on July 11th, 2022, for a total of 370 days of Saildrone deployment, representing *ca*. 10 000 nautical miles (11,933.9 NM). Also, it can be noted that the Saildrone remained 24 hours close to the 0°N-10°W French PIRATA mooring (Figure 2) on February 3rd, 2022, before its travel back towards the United States. The purpose of this operation was to allow for a field intercomparison between instruments. Unfortunately, the CO_2 time series recorded at the French PIRATA mooring was interrupted from September 21th, 2021 to March 8th, 2022 due to a CO_2 sensor issue (Pers. comm. with N.Lefèvre).
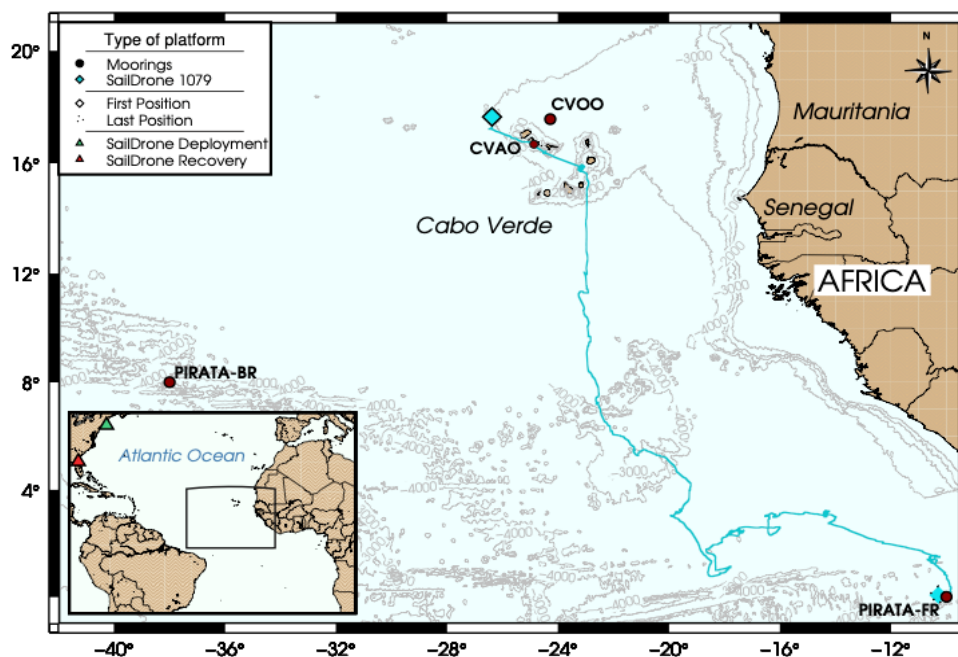

Figure 2. The area of the Eastern Tropical Atlantic Area showing the location of the French (0°N, 10°W) and Brazilian (8°N, 38°W) PIRATA moorings, the Cape Verde Atmospheric Observatory station (CVAO - 16°51'49"N, 24°52'02"W) and the Cape Verde Ocean Observatory station (CVOO - 17.6°N, 24.3°W). The blue line represents the trajectory of the Saildrone from September 2021 to February 2022.

Once the SD was recovered, gross data were downloaded and processed (Sutton et al., 2014). Saildrone Delayed Mode data (high resolution data after recovery of the SD) are available since July 19th, 2022. Table 1 summarises mean values for atmospheric and oceanic parameters that are xCO$_2$, temperature, salinity, chlorophyll-a concentration, or oxygen.

Table 1. Mean values of atmospheric and oceanic xCO2 (μmol mol-1) measurements, zero and span coefficient values (μmol mol-1), seawater temperature (°C), seawater salinity, atmospheric pressure (hPa) and temperature (°C), relative humidity (%), chlorophyll a (μg L-1), oxygen saturation (%) and oxygen concentration (μmol L-1) made by the Saildrone between September 2021 and February 2022. SD stands for Standard Deviation. A distinction has been done between gross data and the one present in the delayed mode dataset. The third column represents the difference between gross data minus delayed mode data.

	Gross Data ± SD	Delayed Mode Data ± SD	Difference (Gross-DM)
xCO2 dry Seawater (μmol mol-1)	408.84 ± 27.66	407.35 ± 27.43	1.49
xCO2 dry Air (μmol mol-1)	412.71 ± 1.88	412.80 ± 1.87	-0.09
Zero Coef. (μmol mol-1)	0.9745 ± 4.9804×10-4	0.9745 ± 5.1529×10-4	0
Span Coef. (μmol mol-1)	0.8903 ± 0.0018	0.8904 ± 0.0019	-0.0001
Temp. Seawater (°)	28.31 ± 0.55	28.24 ± 0.50	0.07
Salinity Seawater	35.14 ± 0.54	35.13 ± 0.46	0.01
Atmo. Pressure (hPa)	1011.2 ± 1.65	1011.2 ± 1.64	0
Atmo. Temp (°)	/	27.51 ± 0.79	/
Relative Humidity (%)	89.75 ± 5.59	89.86 ± 5.59	-0.11
Chlorophyll (μg L-1)	0.43 ± 0.36	0.54 ± 0.44	-0.11
Oxygen saturation (%)	99.82 ± 0.80	99.60 ± 0.84	0.22
Oxygen concentration (μmol L-1)	199.73 ± 1.47	199.54 ± 1.73	0.19

Moreover, one way to evaluate and survey the system's performance, particularly the carbon sensor's, is to look at the calibration results. The SD includes a LICOR system (LI-830) that determines the CO$_2$ gas concentration by measuring the absorption of infrared energy as a sample gas flows through an optical path. The CO$_2$ concentration is based on the difference ratio in the IR absorption between a reference and a sample optical path. The ASVCO2 system on the SD is equipped with on-board reference gas containers to calibrate itself before and after each measurement, and readings of zero gas and reference gas values (that span the ocean pCO$_2$ values of the location where the system is deployed) are made immediately before the calibration. Figure 3 illustrates zero air and span gas coefficient values over the course of the deployment, indicating the system to be very constant and stable, without significant drift over time.
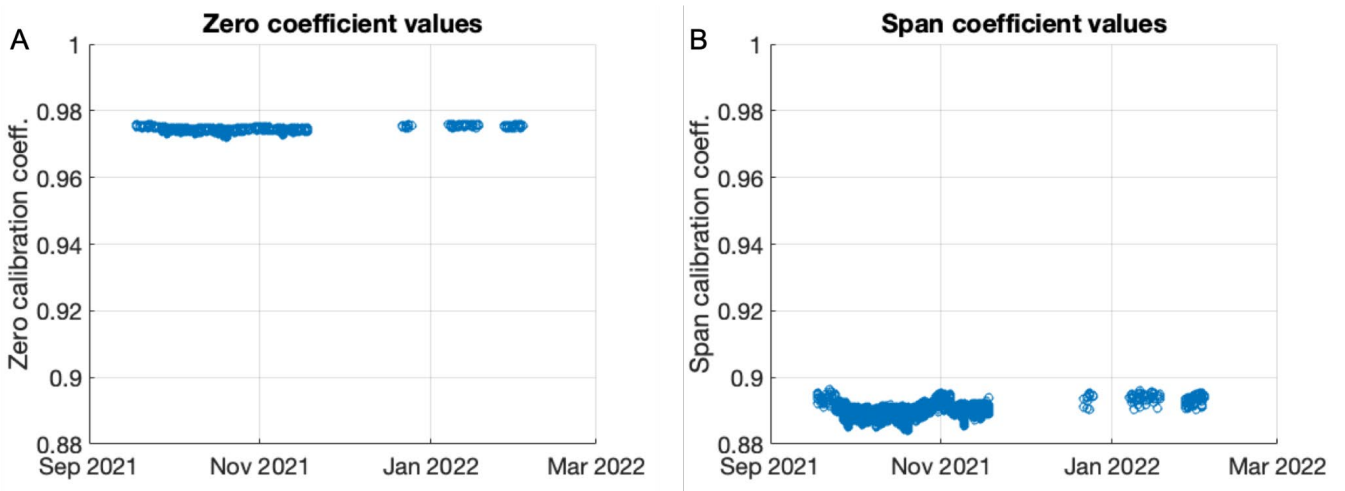
Figure 3. Zero air (A) and span gas (B) coefficient values over the course of the deployment of the Saildrone.

As one of the first field missions utilising the second generation ASVCO2, an issue with CO_2 reference gas flow rate was discovered and adjusted during pre-mission testing. However, given the potential added uncertainty that this issue caused, the estimated measurement uncertainty is likely 3 μmol mol^{-1} during this mission, slightly higher than other ASVCO2 deployments. This estimated uncertainty is consistent with atmospheric and seawater CO_2 validation data comparisons during the mission (see Section 4).

BGC-Argo floats

Five BGC-Argo (equipped with O_2 and pH sensors) deployed during PIRATA FR31 cruise in Spring 2021 are still profiling (Figure 4). They are programmed with a 10 day cycle, 1000 dbar parking depth and profile from their parking depth with a monthly 2000 dbar profile. One float had a complete pH sensor failure 2 months after deployment (6903875, cycle 15); the pH sensor has been remotely turned off, but the remaining sampled variables are still acquired. After drifting almost since its deployment, a second float's pH sensor has been remotely turned off because of sensor failure (6903876, cycle 60 onwards) as of September 2022. Currently, one float's pH sensor is drifting (6903878), but this is correctible in Delayed Mode. Furthermore, as floats 6903876 & 6903877 remained close in space, we can compare their pH during adjustment procedures. BGC Argo floats quality control and adjustment procedures will be detailed in D7.2 "Development of BGCArgo data quality validation based on an integrative multiplatform approach".

For BGC-Argo floats, as of October 24th, 2022:

Table 2. Identification number, date of the first profile, number of cycles (as of October 24th, 2022) and sensor comments for the 5 BGC-Argo floats equipped with pH sensors deployed during the PIRATA cruises, in the framework of EuroSea.

WMO	Date 1st profile (dd/mm/yyyy)	Number of cycles (as of Oct 24th 2022)	Comments
6903874	28/03/2021	71	
6903875	12/03/2021	68	pH sensor failure from cycle 15
6903876	03/04/2021	79	pH drift pH sensor failure from cycle 60

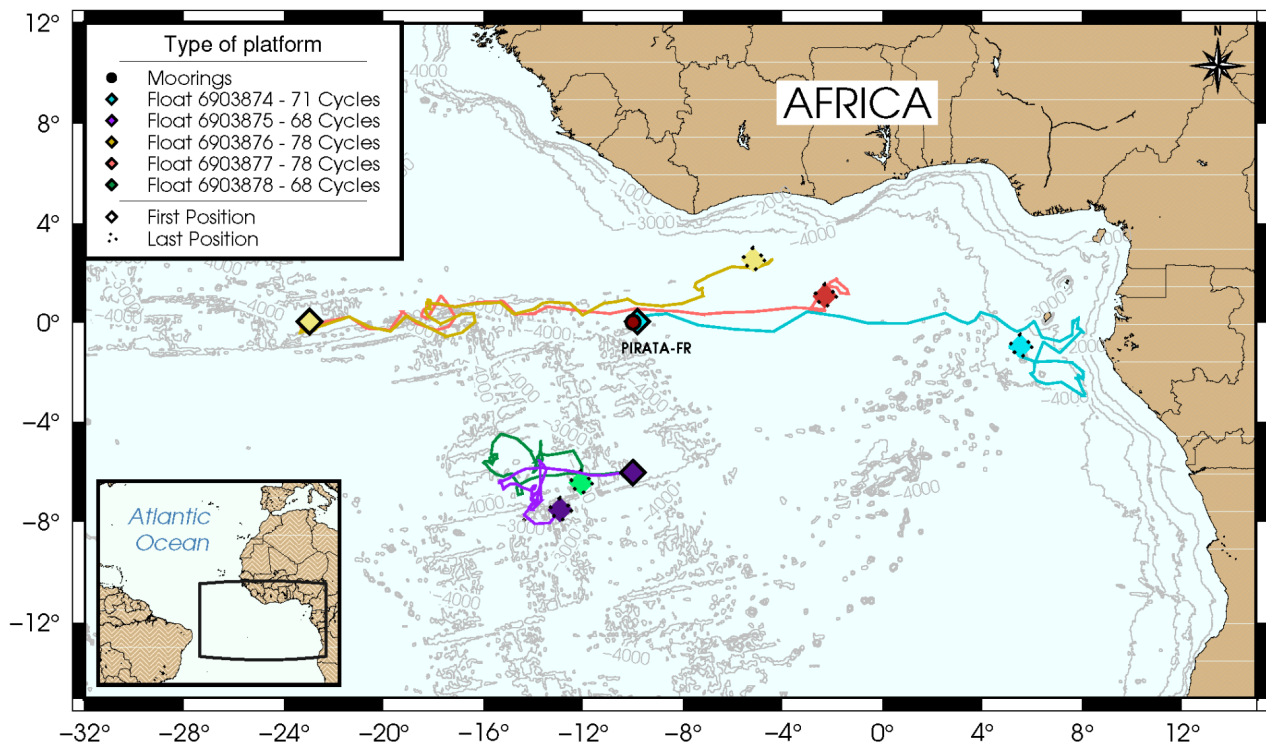| WMO	Date 1st profile (dd/mm/yyyy)	Number of cycles (as of Oct 24th 2022)	Comments
6903877	03/04/2021	79	
6903878	12/03/2021	68	pH drift

Figure 4. Trajectories of the five EUROSEA pH-equipped BGC-Argo floats. Dotted points show the last locations as of October 17th, 2022.

Wave Glider

In the frame of the Autonomous Surface Vehicles (ASV) missions, a Wave Glider vehicle fitted with a VeGAS pCO_2 sensor (Versatile Glider, Atmospheric and Ship pCO_2 high Precision pCO_2 analysers) has been deployed twice, in 2021 and 2022, respectively (Figure 5). This new pCO_2 sensor provides in-air but also in-water measurements. The first Wave Glider deployment was on November 13th, 2021, during the Initiativa Mar Aberto 21.2 cruise on the Portuguese research vessel NRP Dom Carlos I. Measurements started shortly after the deployment and lasted until the recovery on January 26th, 2022.

The second Wave Glider deployment occurred onboard the German research vessel Maria S. Merian during the MSM106 cruise (17°11,183'N - 025°36,098'W) and started to record data on February 25th, 2022. While it stopped acquiring data after 6 days at sea, on March 3rd, 2022, the WaveGlider was recovered on May 23rd, 2022. Figure 5 indicates transects realised by the Wave Glider during each deployment.
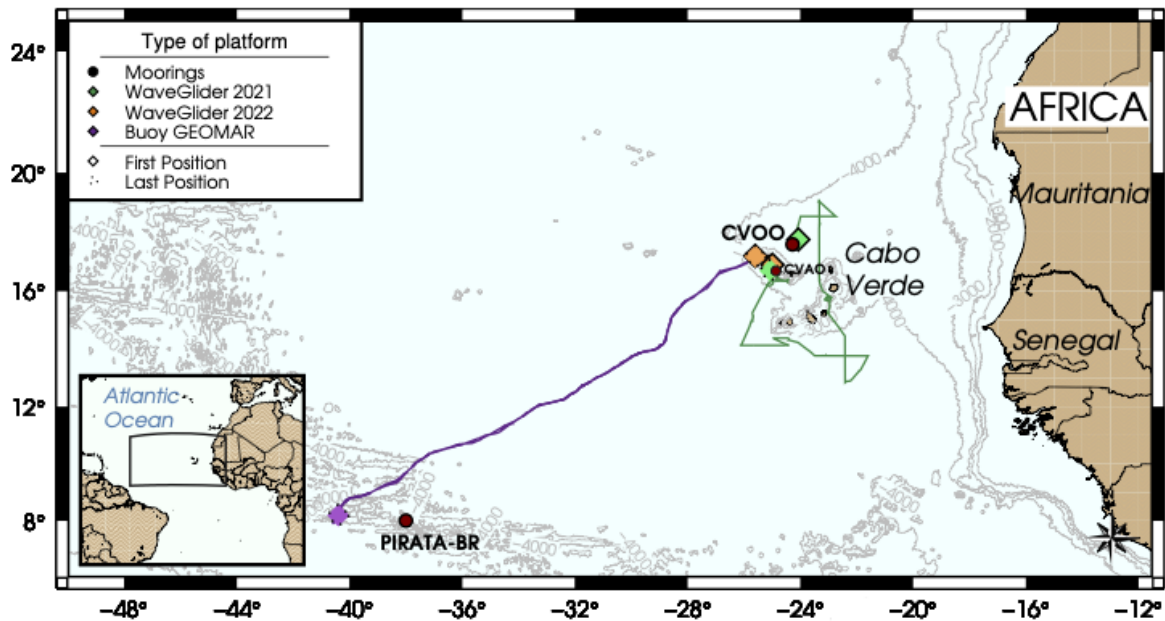
Figure 5. Map of the studied area showing the location of the Cape Verde Atmospheric Observatory station (CVAO - 16°51'49"N, 24°52'02"W), the Cape Verde Ocean Observatory station (CVOO - 17.6°N, 24.3°W), and the Brazilian (8°N, 38°W) PIRATA mooring. The green line shows the Wave Glider positions from November 2021 to January 2022, the orange line represents the transects realised by the Wave Glider between February 2022 and March 2022 and the violet line indicates locations of the GEOMAR buoy deployed in February 2022. The first and final positions of these autonomous platforms are represented by full and dotted symbols, respectively.

The VeGAS pCO_2 sensor, manufactured by Hagan Technologies (Pty) Ltd (Cape Town - South Africa), is based on the infrared (IR) analyser for CO_2 gas detection LICOR (LI-820) linked equilibrator units (Sutton et al., 2014). Following a development stage, all sensors were upgraded, including the LICOR LI-820 being superseded and upgraded to the improved LICOR LI-830. The LI-830 is a non-dispersive infrared sensor that functions by comparing the output of two infrared receivers with selective infrared filters providing CO_2 discrimination. It also contains a pressure sensor in the optical bench and allows the pressure-dependent calculation of CO_2 based on measured infrared absorptance. This system provides data with high accuracy (<2 µatm) and precision (<2 µatm) levels through more effective drying and temperature control, equilibrator design and long-term stability that also reduced the frequency of reference gas calibrations. This system has recently been used for almost two months on a Wave Glider in the Southern Ocean (Nicholson et al., 2022).

GEOMAR Buoy

During the MSM106 cruise that was carried out in the Tropical Atlantic area between February 26th, 2022, and March 19th, 2022, a VeGAS pCO_2 sensor, similar to the one deployed on Wave Glider, has been integrated to the moored GEOMAR buoy and started to record data on February 27th, 2022. This buoy was installed at 17°11'26.34"N - 025°36'0.863"W, northwest of Santo Antao, but started to drift 4 weeks after deployment, on March 22nd, 2022 (Figure 5). The buoy stopped acquiring data after 81 days at sea, on May 23rd, 2022, when it got recovered.

Moreover, before the Wave Glider and the GEOMAR buoy deployments, onboard calibration gas cylinders of these systems were tested and values were determined by comparison with ICOS reference gas with a LICOR 7815. Post-deployment comparison of these cylinders with ICOS reference gas could not be achieved yet because of logistical reasons.

The 8°N, 38°W PIRATA mooring

Since 2008, several deployments of CO_2 sensors have been carried out on the Brazilian (8°N, 38°W) PIRATA mooring (Bourlès et al., 2018). Due to various technical issues but also due to vandalism, long-term CO_2 time series data could not be obtained. In the frame of EuroSea task 7.3, an NKE Instrumentations CARIOCA pCO_2 sensor was thus planned to be installed at this Brazilian mooring. Unfortunately, due to several technical and societal issues, this instrument wasn't deployed at the mooring (see Section 3).

3. Implementation and Current state

The goal of the implementation plan was to develop indicators for carbon fluxes across the air-sea interface based on an improvement of the TAOS observing network. The multi-platform strategy followed in the Eastern Tropical North Atlantic (ETNA) area provided numerous data. In the following sections, only data acquired by autonomous platforms deployed in the frame of the EuroSea project will be presented. We have therefore decided to not explore here CTD casts and SOOP-line datasets as these will be studied deeply in EuroSea deliverable D7.6. Therefore, Table 3 only summarises the number of data points acquired by autonomous surface vehicles and buoys deployed in this region. The number of T, S and O_2 data points for the buoy deployment had to be estimated at an expected minimum, as the final dataset was not available at the time of finalising deliverable 7.1.

*Table 3. Summary of autonomous surface vehicles duration deployments and the parameters measured during each of them. *Number of expected minimum data.*

Platform	pCO_2 sensor type	Measurement Time	Duration (days)	Number of measurements		
				T, S	O_2	xCO_2^{SW}
Saildrone (SD 1079)	ASVCO2 system	Sept. 18th, 2021 - Feb. 3rd, 2022	138	3810929	3810929	2746
Wave Glider 2021	VeGAS pCO_2 sensor	Nov. 13th, 2021 - Jan. 26th, 2022	74	96485	0	5936
Wave Glider 2022	VeGAS pCO_2 sensor	Feb. 26th, 2022 - Mar. 3rd, 2022	6	56734	0	863
GEOMAR buoy	VeGAS pCO_2 sensor	Feb. 27th, 2022 - May 19th, 2022	81	7776*	7776*	7442

To constrain carbon fluxes in this region, ASVs, including Saildrone and Wave Glider platforms equipped with instrumentations for high-quality carbon measurements have been successfully deployed and recovered. Nonetheless, considering the original Saildrone sail plan, we can point out that numerous changes occurred: (1) the sampling frequency for the ASVCO2 system changed numerous times over the Saildrone deployment,

ranging from one measurement every 30 minutes to one every 6 hours, and sometimes even a switch off of the system occurred due to high span gas usage and troubleshoots with the flow, (2) the battery state of charge on SD 1079 took a sharp downturn in January 2022 due to unfavourable conditions. Consequently, the original end date for the 120-day initial mission (January 16th, 2022) was extended, and the Saildrone stopped recording data on February 3rd, 2022. Nevertheless, it should be noted that the technical problems encountered during this deployment have been discussed with the Saildrone team and are easily correctible. This mission has highlighted these points that will be corrected in the future and the interest of these autonomous tools that are easily and remotely manageable. Moreover, as previously stated, the Saildrone remained 24 hours close to the 0°N-10°W French PIRATA mooring on February 3rd, 2022, before starting its transit back to the United States for vehicle retrieval and to allow for a field intercomparison between instruments. Unfortunately, the CO_2 time series recorded at the French PIRATA mooring was interrupted from September 21st, 2021 to March 8th, 2022 due to a CO_2 sensor issue (Pers. comm. with Dr. N.Lefèvre).

In the frame of the ASV missions, a Wave Glider vehicle fitted with VeGAS pCO_2 sensor has been deployed twice, in 2021 and 2022, respectively (Figure 5). During the second Wave Glider deployment, troubleshoots with the flow occurred and only few data have been measured.

At the attached GEOMAR buoy (17°11'26.34"N - 025°36'0.863"W), a VeGAS pCO_2 sensor has also been installed. In comparison to the initial work plan, a technical issue happened on March 22nd, 2022, four weeks after its deployment, as the attached GEOMAR buoy got adrift.

Nevertheless, it can be pointed out that technical sensor installation, deployment, and recovery of these autonomous platforms were well performed. Thus, thanks to these VeGAS pCO_2 sensor deployments, this task will also explore the possibility of integrating this device into existing PIRATA platforms of the TAOS.

In addition, the 8°N, 38°W Brazilian PIRATA mooring was intended to be equipped with an NKE Instrumentations CARIOCA pCO_2 sensor to get CO_2 time series data as the one acquired at the 0°N, 10°W French PIRATA mooring. The COVID pandemic caused multiple delays in purchasing the instrument at IRD and shipping it to Brazil. While the instrument arrived in INPE (Cachoeira Paulista), and successfully functioned in INPE's lab in March 2022, there was, unfortunately, a problem with the CARIOCA sensor onboard during its field phase test (communication test) and therefore it could not be deployed at the mooring (Pers. comm. with Prof. Dr. Leticia Cotrim da Cunha).

Finally, five EuroSea BGC-Argo floats were deployed (see Table 2) between March and April 2021. Out of those 5 floats, 2 pH sensors experienced drift while two had complete pH sensor failure. For float 6903875 in sensor failure, pH values were aberrant from cycle 15 onwards (values up to 30). The pH sensor was therefore turned off after cycle 25 to save battery power. For float 6903876, the pH sensor completely failed from cycle 61 onwards and was therefore turned off a few months later to preserve power.

In addition, thanks to the high degree of coordination between the SD team, Euro-Argo and Principal Investigators within this EuroSea task, an intercomparison experiment has been successfully conducted. By changing the Argo floats' cycling frequency (to daily profiles), profiles from 2 pH-equipped BGC-Argo floats (6903876 & 6903877) were collected on November 15th and 16th 2021 while the Saildrone was circumnavigating around their estimated next ascent profile location (Figure 6).
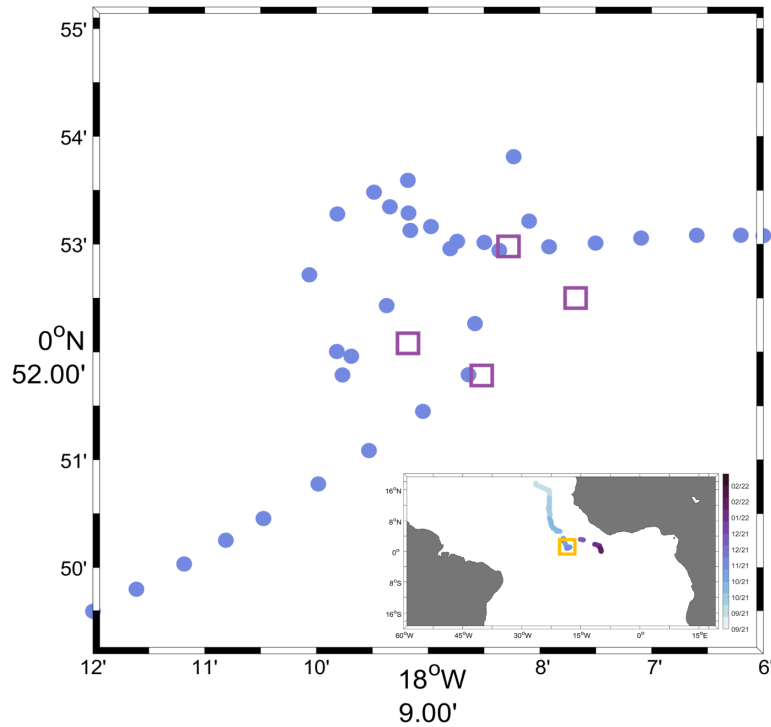
Figure 6. Map of the Saildrone daily measurements (dots) with the Argo profiles (squares) from floats 6903876 and 6903877 used for the matchup around November 16th, 2021. The encased figure on the lower right indicates the location of the focused map in relation to the entire Saildrone mission. The corresponding SD data is mapped according to time.
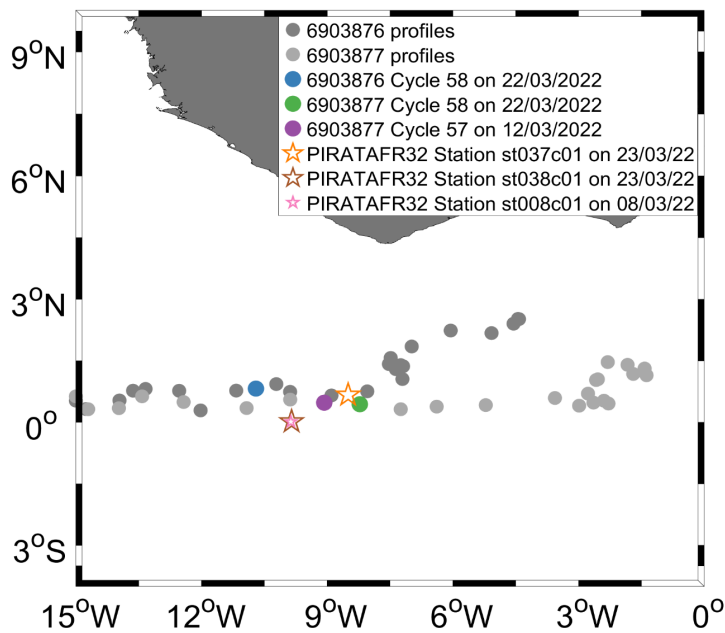

Figure 7. Map of the Argo profiles from floats 6903876 and 6903877 and PIRATAFR32 stations used for the matchup around March 23rd, 2022. Grey and light-grey dots represent Argo profiles and coloured dots (blue for 6903876 and green and purple for 6903877) are the profiles closest in date to the cruise stations. Orange, pink, and brown stars correspond to the PIRATA-FR32 stations with onboard pH measurements on March 23rd, 2022. Note that the pink star is almost superimposed on the brown star, its size has been reduced to improve visibility.

Similarly, a few pH-equipped BGC-Argo float profiles occurred close to the PIRATA-FR32 cruise in March 2022, thanks to the cooperation of the PIRATA team onboard the cruise and in a joint effort with Argo and EuroSea, where *in situ* pH was sampled and analysed onboard for the first time (Figure 7). The Argo profiles were 1-4 days before or after the PIRATA-FR stations (Argo cycles 58 on March 22nd, 2022, vs. stations st037c01 and st038c01 on March 23rd, 2022, and March 24th, 2022; Argo cycle 57 for float 6903877 on March 12th, 2022, vs station st008c01 on March 08th, 2022).

4. Results and lessons learned

4.1. Data consistency: Comparison between different observational platforms

Data quality and consistency can be evaluated through comparisons of CO_2 values acquired in the same time period or spatial scale by other platforms. Thanks to the integrative multi-platform deployment approach followed in the framework of this project, numerous tools and datasets are available to inter-compare the carbon measurements and increase our confidence in them. While seawater xCO_2 comparisons are difficult to interpret considering the high dynamic range and the slow mixing, atmospheric CO_2 comparisons in offshore conditions can provide a better idea of the dataset quality as the atmosphere is well mixed with small changes in space and time (compared to the oceanic reservoir).

The atmospheric xCO_2 values measured in the ETNA area between August 2021 and June 2022 are described in Figures 8A and B with the time series of xCO_2^{ATM} measurements over this period for each autonomous platform. In addition, atmospheric data recorded at the CVAO (Cape Verde Atmospheric Observatory) station have been added (Carpenter et al., 2010). CVAO is an atmospheric monitoring station established to observe the prevailing north-easterly trade winds within the tropics. It is located within 50 metres of the coastline and 10 metres above sea level on the lava-rich island of São Vicente, Cape Verde (16°51'49"N, 24°52'02"W), hence measuring the undisturbed marine boundary layer.

Average xCO_2^{ATM} concentrations recorded in the Eastern Tropical North Atlantic basin of 412.80 ± 1.87 µmol mol^{-1} for the Saildrone, of 419.95 ± 0.63 µmol mol^{-1} for the buoy, of 419.62 ± 1.11 µmol mol^{-1} for the Wave Glider in 2021 and of 422.84 ± 0.38 µmol mol^{-1} for the Wave Glider in 2022 agree with the CVAO mean xCO_2^{ATM} values of 415.64 ± 3.17 µmol mol^{-1} and of 421.04 ± 1.51 µmol mol^{-1} for 2021 and 2022, respectively. The autonomous platforms' data agree well with corrected atmospheric data measured at the CVAO and indicate an increase of the xCO_2^{ATM} content from September to May. Indeed, in the Northern fall, winter, and early spring, plants and soils are taking up less CO_2, causing levels to rise through May. Also, it must be noted that, while data have been recorded in a range of latitude varying from 0°N to *ca*. 18°N, the comparison between each dataset reveals consistent data and highlights the lack of sensitivity of these data to, within reason, latitudinal variations.
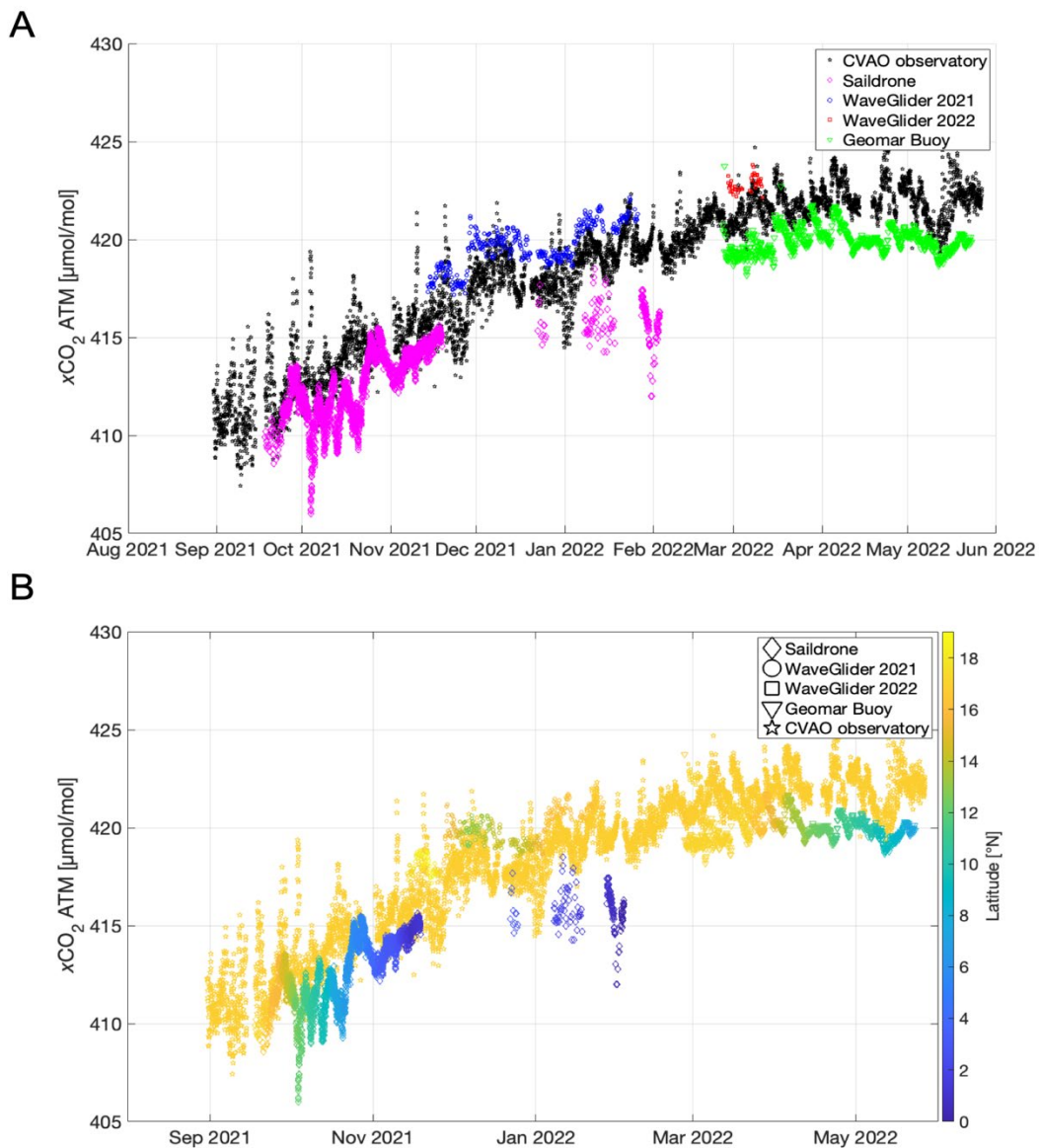
Figure 8. (A and B) Temporal evolution in the Eastern Tropical North Atlantic area of atmospheric xCO₂ values (µmol mol⁻¹) acquired by the Saildrone (diamond dots), the Wave Glider deployed in 2021 (circle dots) and in 2022 (square dots), the GEOMAR buoy (triangle dots) and at the CVAO observatory (stars). In figure B, the colour bar corresponds to the latitude (in °N).

Figure 9A represents the absolute difference between $x\text{CO}_2^{\text{ATM}}$ data recorded at the CVAO observatory and other daily mean $x\text{CO}_2^{\text{ATM}}$ data recorded by autonomous platforms as a function of the distance between the two platforms. As the temporal acquisition resolution was not equal between each platform, atmospheric $x\text{CO}_2$ comparisons were constrained to measurements recorded on the same day. Thus, comparison between mean daily atmospheric CO_2 measurements made from the CVAO station and a distinct platform was possible 70 times for the Wave Glider deployed in 2021, 11 times for the Wave Glider deployed in 2022, 86 times for the Saildrone, and 88 times for the GEOMAR buoy.
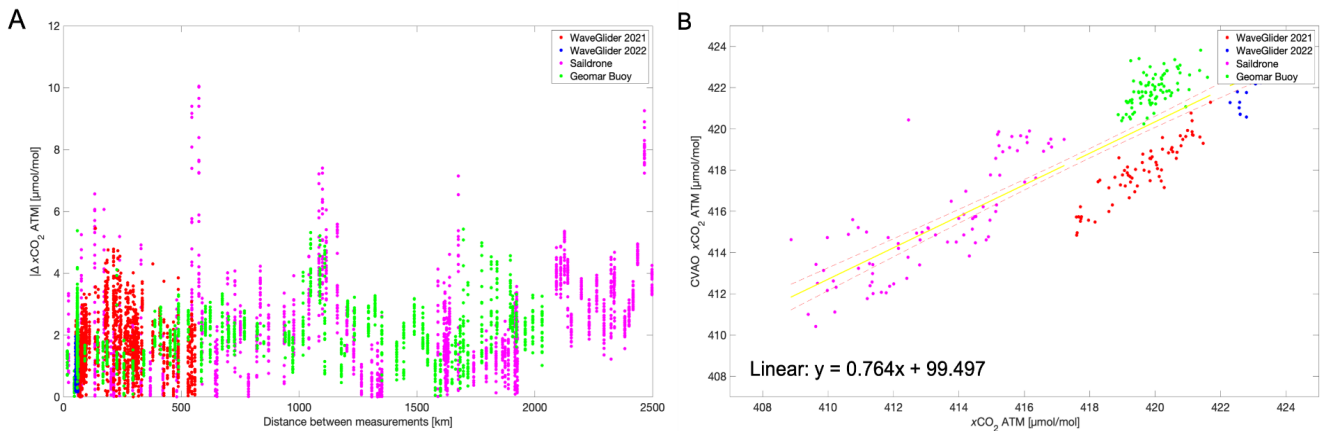
Figure 9. (A) Absolute differences between atmospheric xCO2 data (μmol mol-1) recorded at the CVAO station and daily mean xCO2ATM data acquired by the Wave Glider deployed in 2021 (red dots), the Wave Glider deployed in 2022 (blue dots), the Saildrone (pink dots) and the GEOMAR buoy (green dots) as a function of distance between the two observatory platforms. (B) Daily mean atmospheric xCO2 data (μmol mol-1) recorded at the CVAO station vs. daily mean xCO2ATM data recorded by other autonomous platforms. The colour code for the dots is the same as in Figure 8A.

While the distance between platforms increases, differences show nearly constant values with a mean difference of 2.04 ± 1.41 μmol mol^{-1}, and a peak difference of 10.05 μmol mol^{-1}. It corresponds to the comparison between xCO$_2^{ATM}$ CVAO data and data recorded by the Saildrone. Part of this variability may be explained by the high latitude difference observed between these measurements, and another by the fact that the Saildrone dataset is associated with uncertainties (see Section 3). Nonetheless, the comparison for all platforms showed mean differences ranging between 1.32 and 2.30 μmol mol^{-1}. Moreover, Figure 9B shows that under the constraints previously described, there is a good agreement between daily mean xCO$_2^{ATM}$ data measured at the CVAO station and by other platforms ($R^2 = 0.69$, p-value = 2.35×10^{-63}, N=241). Thus, these comparisons with reference and corrected atmospheric xCO$_2^{ATM}$ data reveal no indication for a pronounced drift or bias in the CO$_2$ sensor response and add confidence in these datasets.

As noted previously, comparing oceanic CO$_2$ data is difficult considering the small time and spatial scales of variability in the ocean. Figures 10A and B represent the temporal evolution of oceanic xCO$_2$ (xCO$_2^{SW}$) data recorded by distinct autonomous platforms between September 2021 and May 2022. Despite the variations in time and spatial scales, xCO$_2^{SW}$ ranged from 346 μmol mol^{-1} (October 2021) to 462 μmol mol^{-1} (October 2021), with comparable means xCO$_2^{SW}$ values of 393.47 ± 5.37 μmol mol^{-1} for the Wave Glider deployed in 2022, of 407.35 ± 27.43 μmol mol^{-1} for the SD, of 399.70 ± 10.45 μmol mol^{-1} for the buoy and of 403.08 ± 11.54 μmol mol^{-1} for the Wave Glider deployed in 2021, respectively.

The highest xCO$_2^{SW}$ value is observed in late summer (October 2021) and, compared to the values observed in September and October 2021, a decreasing trend occurred from December 2021 onward. Thus, even if the latitudinal distribution associated with these data has to be carefully considered, the seasonal variability of xCO$_2^{SW}$ for this area fits well the climatology reported by Fiedler et al. (2013).
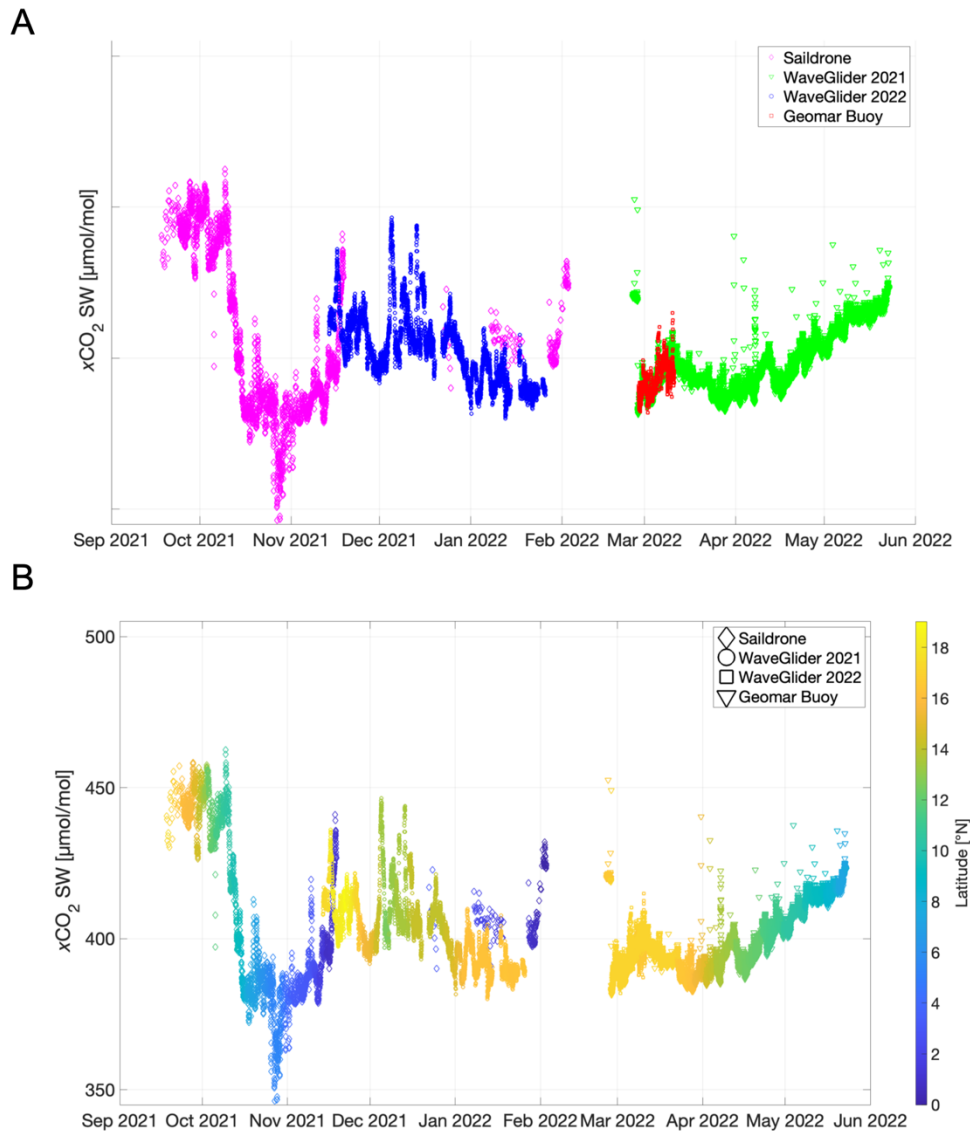
Figure 10. (A and B) Temporal evolution in the Eastern Tropical North Atlantic area of oceanic xCO2 values (µmol mol-1) acquired by the Saildrone (diamond dots), the Wave Glider deployed in 2021 (circle dots) and in 2022 (square dots), the GEOMAR buoy (triangle dots) and at the CVAO observatory (stars). In figure B, the colour bar corresponds to the latitude (in °N). The type of dot used to distinguish each platform is the same as in Figures 8A and B.

Furthermore, other comparisons can be done between data acquisition platforms. In March 2022, the PIRATA-FR32 cruise sampled, for the first time, *in situ* pH onboard. By changing the floats' sampling frequency, onboard pH sampling and analysis close to Argo floats profiles were achieved (Figure 7; 1 to 4 days difference, mean distance 141 km). Indeed, two sampling stations for pH (st037c01 and st038c01) occurred close to cycle 58 of floats 6903876 and 6903877 around March 22nd, and another station (st008c01) was sampled on March 08th, 2022 4 days before cycle 57 of float 6903877 on March 12th. Figure 11 presents the temperature, salinity, O$_2$ and pH measured by the floats during these cycles and the corresponding measurements from PIRATA-FR32 stations. Table 4 details the values of the different variables used for the comparison. The physical parameters show that relatively similar water masses were sampled by both observing platforms with greater differences in surface waters, mainly due to location. Furthermore, there is

17

a good agreement between the corrected pH from the Argo floats and the *in situ* reference data. The mean absolute difference is 0.026. In these comparisons, pH from the Argo floats varies between 7.67 and 8.06 whereas onboard pH spans from 7.72 to 8.01. However, for the matchup around March 22nd, 2022 (first row of Figure 11), BGC-Argo floats only profiled down to 1 000 dbar whereas the *in situ* stations sampled down to 2000 dbar.

Table 4. Mean values of temperature, salinity, dissolved oxygen and pH measurements made by the BGC-Argo floats on the profiles selected for the comparison, the corresponding shipborne data and the difference. SD stands for Standard Deviation. Dissolved oxygen and pH were adjusted following BGC-Argo quality control procedures.

		Float±SD	Shipborne±SD	Mean absolute difference±SD	Date difference (days)	Distance difference (km)
6903876 cycle 58 vs PIRATAFR32 station 37	Temperature	15.76±7.63	13.63±9.07	0.82±0.96	1.7	245.3
	Salinity	35.17±0.49	35.25±0.54	0.12±0.14		
	O_2	141.67±35.97	153.02±51.36	10.66±6.79		
	pH	7.90±0.097	7.87±0.101	0.023±0.017		
6903876 cycle 58 vs PIRATAFR32 station 38	Temperature	15.76±7.63	13.63±9.07	0.51±0.42	2.1	129.3
	Salinity	35.17±0.49	35.25±0.54	0.06±0.07		
	O_2	141.67±35.97	153.02±51.36	8.18±4.77		
	pH	7.90±0.097	7.87±0.101	0.023±0.0207		
6903877 cycle 58 vs PIRATAFR32 station 37	Temperature	15.87±7.42	13.75±9.28	0.78±0.80	1.7	39.8
	Salinity	35.36±0.49	35.23±0.63	0.17±0.21		
	O_2	143.44±38.24	155.79±53.14	9.89±7.35		
	pH	7.91±0.105	7.88±0.110	0.023±0.0238		
6903877 cycle 58 vs PIRATAFR32 station 38	Temperature	15.87±7.42	13.75±9.28	1.02±1.21	2.1	187
	Salinity	35.36±0.49	35.23±0.63	0.16±0.22		
	O_2	143.44±38.24	155.79±53.14	14.80±9.59		

		Float±SD	Shipborne±SD	Mean absolute difference±SD	Date difference (days)	Distance difference (km)
	pH	7.91±0.105	7.88±0.110	0.038±0.0383		
6903877 cycle 57 vs PIRATAFR32 station08	Temperature	14.88±8.02	12.94±8.97	0.61±0.63	4	102.2
	Salinity	35.25±0.49	35.27±0.62	0.10±0.10		
	O_2	148.27±46.20	164.03±46.51	13.26±8.00		
	pH	7.91±0.100	7.89±0.096	0.023±0.0196		
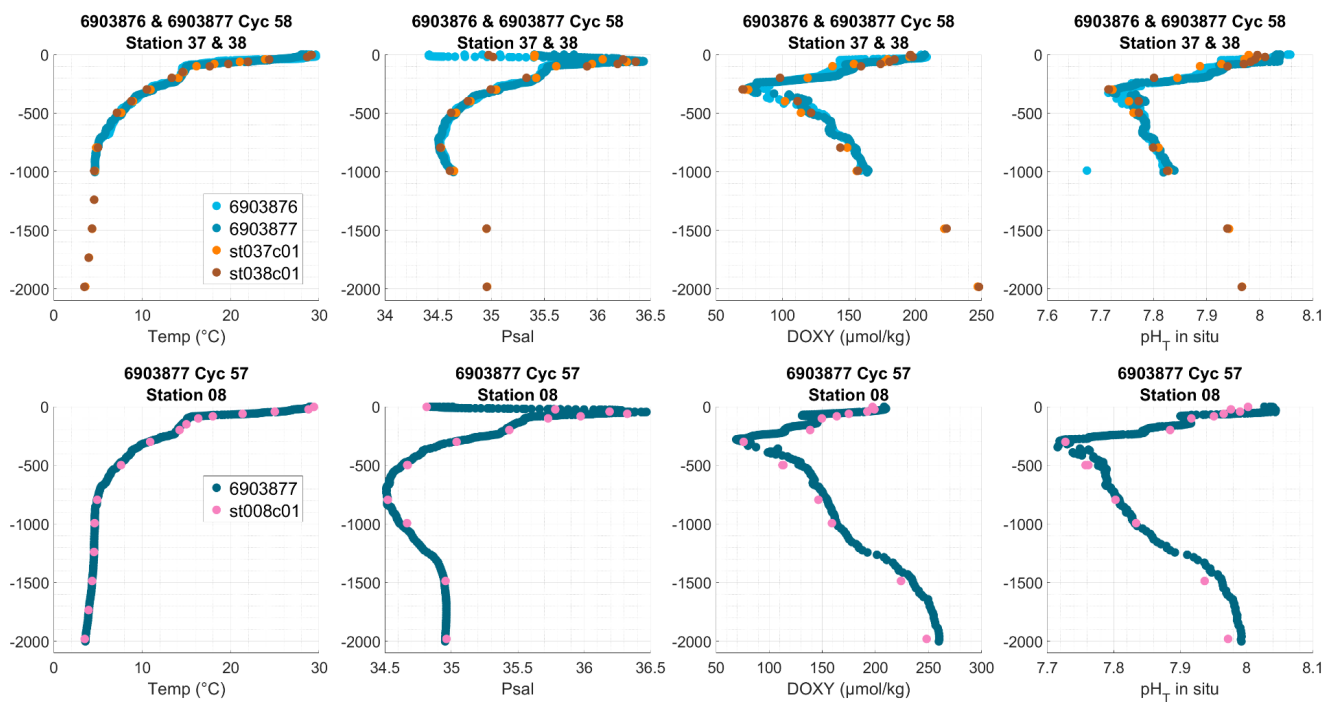
Figure 11. Profiles of temperature, salinity, dissolved oxygen and in situ pH from Argo floats cycles and stations from the PIRATAFR32 cruise. Dissolved oxygen and pH were adjusted following BGC-Argo quality control procedures.

Lastly, while BGC-Argo floats do not directly measure pCO$_2$, from their pH measurement and neural network derived TA, pCO$_2$ can be derived using the properties of the carbonate system. By changing the floats' sampling frequency, Saildrone pCO$_2$ measurements close to Argo floats profiles were achieved. Therefore, at the location and time of the crossover between the BGC-Argo floats and the Saildrone, pCO$_2$ was computed using adjusted Argo pH (using the SAGE tool, Maurer et al., 2021) and TA computed using the ESPER (Carter et al., 2021) neural-network-based method (specifically using the mixed version, which combines MLR and neural network outputs). Figure 12 presents the comparison between the Argo-derived pCO$_2$ and the Saildrone's pCO$_2$ time series. The BGC-Argo-derived pCO$_2$ matches the Saildrone's values reasonably well.

There was high variability in a relatively small-time frame in the Saildrone's pCO_2 and this is also reproduced in the BGC-Argo measurements. This might be due to the sharp decrease in temperature at that time (loss of 1°C in SST in a few days). Note that the estimated uncertainty associated with the pCO_2 computed with CO2SYS (van Heuven et al., 2011) from BGC-Argo float's pH and neural-network-based TA (Carter et al., 2021) is 14 μatm (through propagation of errors in the carbonate system).
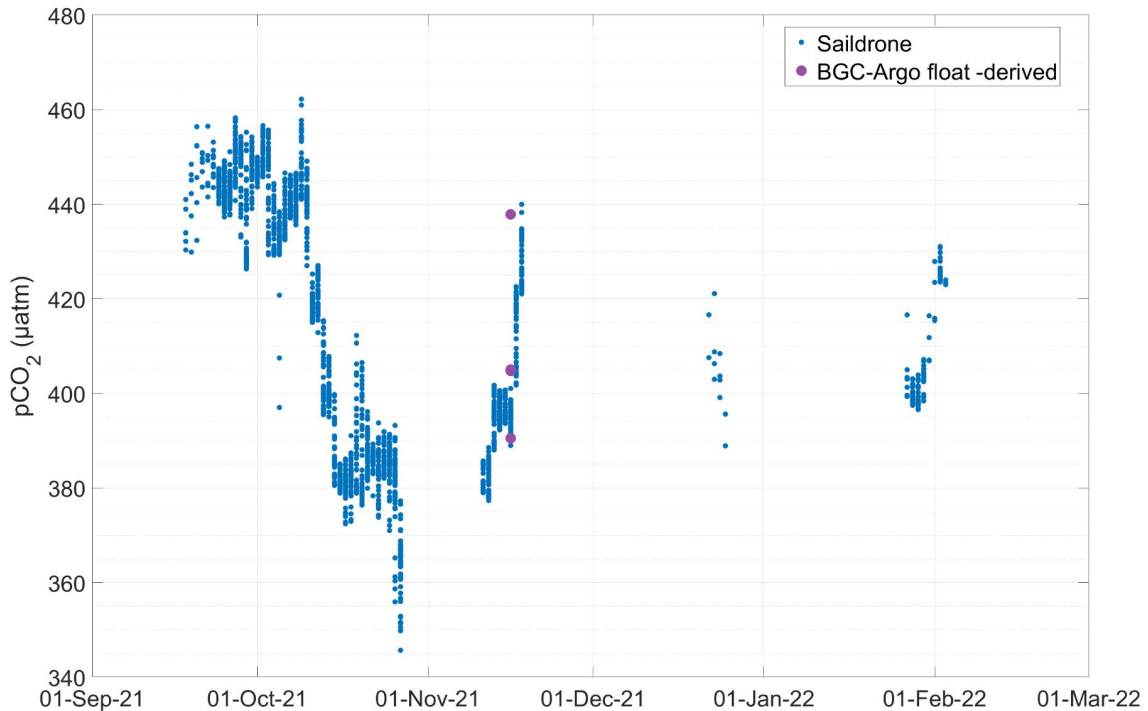

Figure 12. Saildrone seawater pCO2 time series (blue) and pCO2 derived from BGC-Argo float's pH and neural-network based TA (purple).

4.2. Air-sea fluxes

Air-sea CO_2 fluxes in the Eastern Tropical North Atlantic basin have been calculated from seawater and atmospheric xCO_2 values measured by the Saildrone. The conversion of xCO_2 (mole fraction of CO_2 in μmol mol^{-1}) into pCO_2 (partial pressure of CO_2, in μatm) was done using atmospheric data and biogeochemical parameters recorded by the Saildrone (*i.e.*, relative humidity (in %), atmospheric partial pressure (in atm), temperature (in °C) and salinity). Then, air-sea CO_2 fluxes have been calculated according to the equation described in Wanninkhof et al. (2014), with wind speed measurements acquired by the Saildrone 5 meters above the sea surface level. The flux of CO_2 expressed hereafter is in mmol m^{-2} day^{-1}. By convention, a negative sign indicates a flux from the atmosphere to the ocean. A detailed description of methodologies followed to convert xCO_2 values and to calculate air-sea CO_2 fluxes can be found in the Supplementary Material. In the following, only CO_2 flux data from the accomplished Saildrone mission will be presented and discussed. A more integrative assessment at higher spatial range (basin-wide) including a cost/benefit assessment will be addressed in the EuroSea D7.6 deliverable.
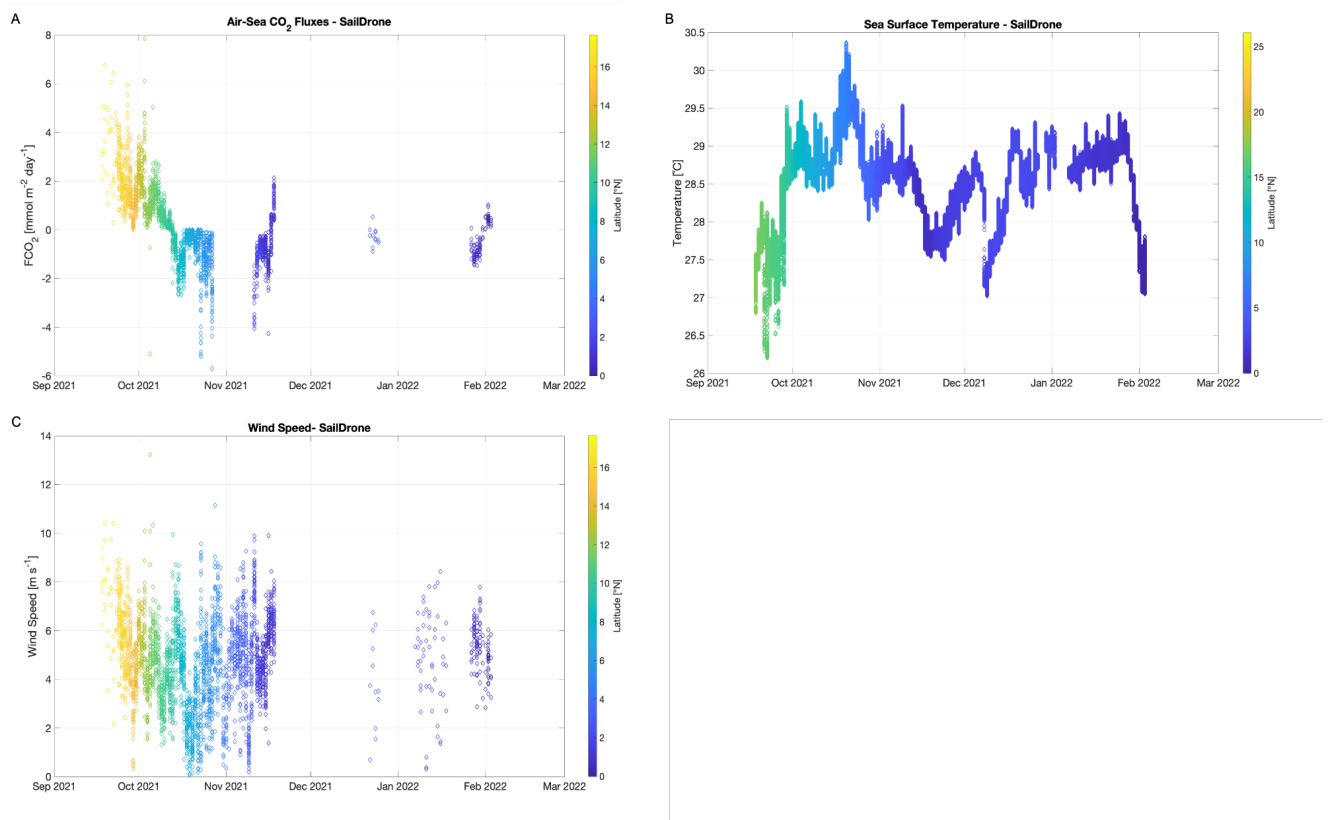
Figure 13. Time-series observations for air-sea CO_2 fluxes (mmol m^{-2} day^{-1} - A), sea surface temperature (°C - B) and wind speed (m s^{-1} - C) measured and calculated based on the data acquired by the Saildrone deployed in the ETNA area from September 2021 to February 2022. By convention, a negative flux indicates fluxes directed from the atmosphere to the ocean, and a positive flux indicates fluxes directed from the ocean to the atmosphere.

Estimated daily CO_2 fluxes in this area varied between -5.70 and 7.86 mmol m^{-2} d^{-1} over the studied period, for a mean value of -0.21 ± 1.55 mmol m^{-2} d^{-1}. Positive values have been measured from September 2021 to October 2022, while negative values have been calculated during the remaining recorded period (Figure 13A). Thus, the daily CO_2 flux in this area is lower in winter (November-February) and higher in summer (September-October) but does not follow the general temporal variability of sea surface temperature in this region (Figure 13B). The CO_2 flux is mainly influenced by the difference of $x$$CO_2$ between the ocean and the atmosphere (Figure not shown).

From September to February, wind speed was relatively stable, and values ranged from 0.07 to 13.23 m s^{-1}, for a mean value of 4.69 ± 1.80 m s^{-1} (Figure 13C). The highest values have been measured between September and November, at the end of summer, followed by a decrease in wind intensity in January-February. As the wind intensity was high in October 2021, absorption of CO_2 strongly increased during this part of the year, even if high temperatures were measured. Indeed, temperature, through its control on the solubility of CO_2, hence the seawater $p$$CO_2$, might drive the magnitude of the difference between oceanic and atmospheric $p$$CO_2$. But negative fluxes calculated in November and associated with seawater warming leading to a significant reduction of atmospheric CO_2 absorption reveals that other processes might occur in this region.

Nevertheless, even if entire annual seawater and atmospheric pCO_2 cycles have not been recorded by the Saildrone, the climatological sink of CO_2 observed in the Eastern Tropical North Atlantic basin during the last months of the year in this study is corroborated by other studies. In the Tropical North Atlantic region (0–30°N, 70–15°W), Lefèvre et al. (2019) measured a mean annual flux, over the period 2006-2014 of 0.31 mmol m^{-2} d^{-1}, with an area being alternatively a source (in summer) or sink (in winter) for atmospheric CO_2. In the North Equatorial Atlantic area, Padin et al. (2010) reported air-sea CO_2 fluxes varying between −0.7 ± 0.4 mol m-2 y^{-1} in spring and 0.0 ± 0.5 mol m^{-2} y^{-1} in autumn. From September to February, the average flux of -0.21 ± 1.55 mmol m^{-2} d^{-1} (-0.08 ± 0.57 mol m^{-2} y^{-1}) calculated in this study is in agreement with previously recorded fluxes.

4.3.   Drivers of the oceanic pCO_2 variability

In the ocean, spatial and temporal variability of the xCO_2 is due to concomitant biological and physical processes. Based on the thermodynamic effect of temperature on the solubility of dissolved CO_2 in seawater (4.23% change per 1°C; Takahashi et al., 1993, 2002), contributions of thermal (xCO_2^{TD}) and non-thermal (xCO_2^{N}) processes, including biological activity but also air-sea exchanges, advection, and vertical diffusion, have been calculated based on the SD dataset. This procedure (and the hereafter section), while being at the edge of the scope of this deliverable, gives us confidence in our dataset as it allows a comparison, through another angle, of the dataset to the literature. A detailed description of the methodology followed to determine xCO_2^{N} and xCO_2^{TD} can be found in the Supplementary Material.

Figure 14 represents changes, over the studied period, of CO_2 molar fraction induced by temperature and non-thermal effects in the Eastern Tropical North Atlantic. In this region, the main variation of xCO_2^{SW} occurs because of changes induced by non-thermal processes, with a contribution to the changes xCO_2^{SW} ranging from -64.66 µmol mol^{-1} to 69.06 µmol mol^{-1}. Based on the observed relationship between xCO_2^{SW} and xCO_2^{N}, non-thermal processes explain almost entirely the xCO_2^{SW} variability, with a R^2 value of *ca*. 0.93 (Table 5). Conversely, the xCO_2^{TD} variability due to thermal processes varied between -38.34 µmol mol^{-1} and 31.92 µmol mol^{-1}.

In most oceanic areas, the seawater pCO_2 seasonality, and thus by extension the xCO_2^{SW} seasonality, is mainly driven by temperature changes, and secondary by DIC and AT changes (*e.g.,* Takahashi et al., 1993). In the studied area, this statement must be revised in the light of the important effect of salinity variations on the xCO_2^{SW}. Indeed, based on the observed relationships between xCO_2^{SW}, xCO_2^{N} and sea surface salinity (SSS - Table 5), salinity changes explain more than 70% and 74% of the xCO_2^{N} and xCO_2^{SW} variabilities in the area, respectively. This pattern has already been reported in the North Equatorial Counter Current province (8°-1°N), where Padin et al. (2010) stated that the influence of SSS on seawater fugacity (fCO_2^{SW}) reached a maximum value of 79% in this area, with a coefficient of 17.3 ± 0.3 µatm per SSS unit. At the PIRATA buoy located 6°S - 10°W, Lefèvre et al. (2016) reported on seasonal timescales, a correlation between seawater fCO_2 and sea surface salinity. Moreover, in the Eastern North Atlantic region (35°W - 10°W / 30°N - 55°N), Lüger et al. (2004) reported that, while depending on the mixed layer depth, the seawater pCO_2 variability is dominated by non-temperature effects.
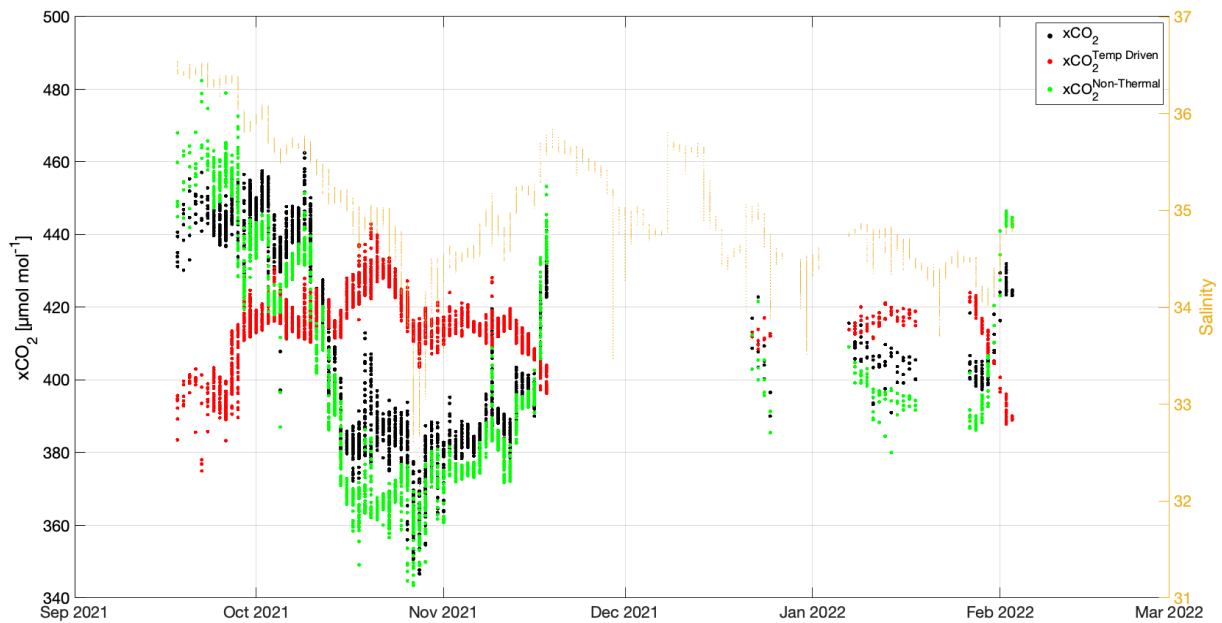
Figure 14. Temporal evolution of surface seawater xCO_2 changes induced by thermal variations (xCO_2^{TD}, red dots), surface seawater xCO_2 changes induced by non-thermal processes (xCO_2^N, green dots), surface seawater xCO_2 (black dots) and salinity (orange dots) in the Eastern Tropical North Atlantic area based on the Saildrone dataset deployed from September 2021 to February 2022.

Table 5. Regression coefficients and xCO_2^{SW} and xCO_2^N variabilities explained by xCO_2^{SW}, xCO_2^N and sea surface salinity (SSS). The correlation coefficient (R^2) and p-value are also given. N stands for the number of data included in each analysis.

	Relationship	p-value	R^2	N
xCO_2^{SW} vs. xCO_2^N	1.1027x - 48.66	<0.05	0.927	2744
SSS vs. xCO_2^{SW}	31.77x -708.27	<0.05	0.745	2744
SSS vs. xCO_2^N	35.434x -843.90	<0.05	0.705	2744

During its deployment, the SD crossed numerous biogeochemical and hydrological provinces impacted by distinct currents. Indeed, along the transect realised by the Saildrone, temperature and salinity values appeared to be anti-correlated, with the highest salinity values recorded in the Northern part of the region and the lowest in the Southern part, and conversely for the temperature. All these rapid and high fluctuations of both sea surface temperature and salinity (and also xCO$_2^{SW}$) suggest that horizontal rather than vertical processes are present in this region. Due to its connection with the subtropical Atlantic region and also the North Atlantic Subtropical gyre, the studied Eastern Tropical North Atlantic area combines different circulation features. North of the studied area, the Canary Current and the North Equatorial Current are salty and cold surface currents define the eastern and southern dynamic boundaries of the North Atlantic Subtropical Gyre (Hernández-Guerra et al., 2005). Then, North of the equator, low sea surface salinity values characterise the surface waters of the North Equatorial Counter Current (Richardson and Reverdin, 1987). In

this province, the seasonal variability of sea surface temperature reached the highest value in the boreal autumn season (Padin et al., 2010).

Conclusions

This deliverable describes the successful multi-platform deployment and intercomparison approach followed in the Eastern tropical Atlantic region in response to the growing and urgent demand for sustained observations of oceanic carbon data in response to human pressure and global climate change. The report describes in detail how EuroSea fulfilled its Task 7.3 by deploying numerous autonomous tools (Saildrone, Wave Glider, attached buoy, BGC-Argo floats) equipped with diverse sensors and systems (pH sensor, VeGAS pCO$_2$ sensor, ASVCO2 sensor, IFSET pH measurement technology). Thanks to collaborations with international institutions, the optimization of the existing Tropical Atlantic Observing System has been initiated and the capacity to address different elements for monitoring tropical carbon variations has increased. While there is still an issue with one pCO$_2$ sensor deployment at the PIRATA 8°N, 38°W mooring, key collaborations were initiated through this work, and a future implementation can still be considered. Using new technologies such as the Saildrone platform or the new VeGAS pCO$_2$ sensor, this task has raised the possibility of implementing these tools as new services to explore this area and strengthen the global ocean observing system. Even if the results presented in this report must be carefully interpreted as they are still preliminary, the comparison between different observational platforms revealed an important consistency and gives us confidence in the quality of the data. Nevertheless, it should also be pointed out that oceanographic cruises and data acquired through classical observing systems (including SOOP-line) remain the reference tool to obtain high-quality data to then compare autonomous platform datasets. Furthermore, in cases where multiple stakeholders with overlapping data interests can be served by such a multi-integrated platform approach, operating expenses can be distributed among the group, further increasing cost-efficiency for all.

This deliverable also describes significant progress towards establishing a procedure to compare and correct data. Indeed, this report highlights that the strategy followed in this region, based on the synergic combination of multiple platforms, allows data intercomparison thereby reducing uncertainties and adding confidence to the datasets. Further work is required to deliver internationally agreed operating and comparison protocols to then obtain high-quality carbon data to accurately estimate oceanic changes in this area.

A more detailed assessment on the quality enhancement of carbon fluxes in the tropical Atlantic will be provided in EuroSea deliverable D7.6, to be submitted in 2023.

Data availability statement

Fully processed and finalised data will be submitted in 2023 to the Surface Ocean CO_2 Atlas (SOCAT) for community-based quality control and final ingestion into global carbon synthesis products and assessments. Argo data are available at http://doi.org/10.17882/42182#96550 or at ftp://ftp.ifremer.fr/ifremer/argo/dac/coriolis. These data were collected and made freely available by the International Argo Program and the national programs that contribute to it (https://argo.ucsd.edu, https://www.ocean-ops.org). The Argo Program is part of the Global Ocean Observing System. Atmospheric data recorded at the CVAO station are available at https://catalogue.ceda.ac.uk/uuid/81693aad69409100b1b9a247b9ae75d5. Data from the French PIRATA cruises are available on the SEANOE website (https://www.seanoe.org).

Acknowledgements

References

Bittig, H. C., Maurer, T. L., Plant, J. N., Schmechtig, C., Wong, A. P. S., Claustre, H., Trull, T. W., Udaya Bhaskar, T. V. S., Boss, E., Dall'Olmo, G., Organelli, E., Poteau, A., Johnson, K. S., Hanstein, C., Leymarie, E., Le Reste, S., Riser, S. C., Rupan, A. R., Taillandier, V., … Xing, X., 2019. A BGC-Argo Guide: Planning, Deployment, Data Handling and Usage. *Frontiers in Marine Science*, 6.

Boers, N., 2021. Observation-based early-warning signals for a collapse of the Atlantic Meridional Overturning Circulation. *Nature Climate Change*, 11, 21.

Bourlès, B., Brandt, P., Lefèvre, N. and Hahn, J., 2018. AtlantOS EU H2020 633211 Deliverable 3.9 "PIRATA data system upgrade report : Technical report mostly related to biogeochemical sensors (O_2 and CO_2 sensors) data, their real-time transmission and O_2 and CO_2 data control quality and their integration to existing systems, in relation with the WP7", https://doi.org/10.3289/AtlantOS_D3.9.

Bourlès, B., Araujo, M., McPhaden, M. J., Brandt, P., Foltz, G. R., Lumpkin, R., Giordani, H., Hernandez, F., Lefèvre, N., Nobre, P., Campos, E., Saravanan, R., Trotte-Duhà, J., Dengler, M., Hahn, J., Hummels, R., Lübbecke, J. F., Rouault, M., Cotrim, L., … Perez, R. C., 2019. PIRATA: A Sustained Observing System for Tropical Atlantic Climate Research and Forecasting. *Earth and Space Science*, 6(**4**): 577-616.

Brüchert, V., Currie, B., Peard, K. R., Lass, U., Endler, R., Dübecke, A., et al., 2006. Biogeochemical and physical control of shelf anoxia and water column hydrogen sulphide in the Benguela coastal upwelling system, in Past and Present Water Column Anoxia, ed. L. N. Neretin (New York, NY: Springer), 161–193.

Carpenter, L.J., Hopkins, J.R., Lewis, A.C., Neves, L.M., Moller, S., Pilling, M.J., Read, K.A., Young, T.D., Lee, J.D., 2010. Continuous Cape Verde Atmospheric Observatory Observations. NCAS (National Centre for Atmospheric Science) British Atmospheric Data Centre. http://catalogue.ceda.ac.uk/uuid/81693aad69409100b1b9a247b9ae75d5.

Carter, B. R., Bittig, H. C., Fassbender, A. J., Sharp, J. D., Takeshita, Y., Xu, Y., et al., 2021. New and updated global empirical seawater property estimation routines. *Limnology and Oceanography: Methods*, 19(**12**), 785–809.

Chang, P., Fang, Y., Saravanan, R., Ji., L. and Seidel, H., 2006. The cause of the fragile relationship between the Pacific El Niño and the Atlantic Niño. *Nature*, 443: 324-328.

Chen, C. T. A., and Borges, A. V., 2009. Reconciling opposing views on carbon cycling in the coastal ocean: continental shelves as sinks and near-shore ecosystems as sources of atmospheric CO_2. *Deep Sea Res. II* 56: 578–590.

Czaja, A., van der Vaart, P. and Marshall, J., 2002. A diagnostic study of the role of remote forcing in tropical Atlantic variability. *J. Clim.* 15: 3280–3290.

Dickson, A. G., C. L. Sabine, and J. R. Christian (Eds.), 2007. Guide to Best Practices for Ocean CO_2 Measurements. PICES Special Publication 3, 191 pp.

Durack, P. J., Wijffels, S. E., and Matear, R. J., 2012. Ocean salinities reveal strong global water cycle intensification during 1950 to 2000. *Science*, 336: 455–458.

Fiedler, B., Fietzek, P., Vieira, N., Silva, P., Bittig, H. C., & Körtzinger, A., 2013. In Situ CO_2 and O_2 Measurements on a Profiling Float. Journal of Atmospheric and O*ceanic Technology*, *30* (**1**): 112-126.

Foltz, G.R., et al., 2019. The Tropical Atlantic Observing System. *Frontiers in Marine Science*, 6: 1-36.

Goni, G., Roemmich, D., Molinari, R., Meyers, G., Sun, C., Boyer, T., Baringer, M., Gouretski, V., DiNezio, P., Reseghetti, F., Vissa, G., Swart, S., Keeley, R., Garzoli, S., Rossby, T., Maes, C. and Reverdin, G., 2010. The Ship of Opportunity program, Proceedings of OceanObs'09: Sustained Ocean Observations and Information for Society, (Vol. 2). Venice, Italy: ESA Publication.

Hernández-Guerra, A., Fraile-Nuez, E., López-Laatzen, F., Martínez, A., Parrilla, G., & Vélez-Belchí, P., 2005. Canary Current and North Equatorial Current from an inverse box model. *Journal of Geophysical Research: Oceans*, 110 (**C12**).

Johnson, K. S., Plant, J. N., Coletti, L. J., Jannasch, H. W., Sakamoto, C. M., Riser, S. C., et al., 2017. Biogeochemical sensor performance in the SOCCOM profiling float array. *Journal of Geophysical Research: Oceans*, 122(**8**), 6416–6436.

Karstensen, J., Stramma, L., and Visbeck, M., 2008. Oxygen minimum zones in the eastern tropical Atlantic and Pacific. *Prog. Oceanogr*. 77: 331–350.

Landschützer, P., Gruber, N., Bakker, D. C. E., and Schuster, U., 2014. Recent variability of the global ocean carbon sink. *Glob. Biogeochem. Cycles* 28: 927–949.

Lefèvre, N., Veleda, D., Araujo, M., & Caniaux, G., 2016. Variability and trends of carbon parameters at a time series in the eastern tropical Atlantic. *Tellus B: Chemical and Physical Meteorology*, 68 (**1**): 30305.

Lefèvre, N., Veleda, D., Tyaquiçã, P., Perruche, C., Diverrès, D., & Ibánhez, J. S. P., 2019. Basin-Scale Estimate of the Sea-Air CO_2 Flux During the 2010 Warm Event in the Tropical North Atlantic. *Journal of Geophysical Research: Biogeosciences*, 124 (**4**): 973-986.

Lüger, H., Wallace, D. W. R., Körtzinger, A., & Nojiri, Y., 2004. The *p*CO_2 variability in the midlatitude North Atlantic Ocean during a full annual cycle. *Global Biogeochemical Cycles*, 18 (**3**).

Machu, E., Capet, X., Estrade, P. A., Ndoye, S., Brajard, J., Baurand, F., et al., 2019. First evidence of anoxia and nitrogen loss in the Southern Canary upwelling system. *Geophys. Res. Letters*, 46: 2619–2627.

Manley, J. and Willcox, S., 2010. The Wave Glider: A persistent platform for ocean science, OCEANS'10 IEEE SYDNEY, pp. 1-5.

Martz, T., Daly, K., Byrne, R., Stillman, J. and Turk, D., 2015. Technology for Ocean Acidification Research: needs and availability. *Oceanography*, 25:40–7.

Maurer, T. L., Plant, J. N., & Johnson, K. S., 2021. Delayed-mode quality control of oxygen, nitrate and pH data on SOCCOM biogeochemical profiling floats. *Front. Mar. Sci.,* 8:683207.

Meinig, C., Burger, E.F., Cohen, N., Cokelet, E.D., Cronin, M.F., Cross, J.N., de Halleux, S., Jenkins, R., Jessup, A.T., Mordy, C.W., et al., 2019. Public–Private Partnerships to Advance Regional Ocean-Observing

Capabilities: A Saildrone and NOAA-PMEL Case Study and Future Considerations to Expand to Global Scale Observing. *Frontiers in Marine Science*, 6: 448.

Nicholson, S.-A., Whitt, D. B., Fer, I., du Plessis, M. D., Lebéhot, A. D., Swart, S., Sutton, A. J., & Monteiro, P. M. S., 2022. Storms drive outgassing of CO_2 in the subpolar Southern Ocean. *Nature Communications*, 13(**1**): 158.

Padin, X. A., Vázquez-Rodríguez, M., Castaño, M., Velo, A., Alonso-Pérez, F., Gago, J., Gilcoto, M., Álvarez, M., Pardo, P. C., de la Paz, M., Ríos, A. F., & Pérez, F. F., 2010. Air-Sea CO_2 fluxes in the Atlantic as measured during boreal spring and autumn. *Biogeosciences*, 7 (**5**): 1587-1606.

Parard, G., Lefèvre, N., & Boutin, J., 2010. Sea water fugacity of CO_2 at the PIRATA mooring at 6°S, 10°W. *Tellus B: Chemical and Physical Meteorology*, 62 (**5**), 636-648.

Richardson, P.L., & Reverdin, G., 1987. Seasonal cycle of velocity in the Atlantic North EquatorialCountercurrent as measured by surface drifters, current meters, and ship drifts. *Journal of Geophysical Research*, 92 (**C4**), 3691.

Sabine, C., Sutton, A., McCabe, K., Lawrence-Slavas, N., Alin, S., Feely, R., Jenkins, R., Maenner, S., Meinig, C., Thomas, J., van Ooijen, E., Passmore, A., & Tilbrook, B., 2020. Evaluation of a New Carbon Dioxide System for Autonomous Surface Vehicles. *Journal of Atmospheric and Oceanic Technology,* 37 (**8**), 1305-1317.

Servain, J., Caniaux, G., Kouadio, Y. K., McPhaden, M. J., and Araujo, M., 2014. Recent climatic trends in the tropical Atlantic. *Clim. Dyn*. 41: 3071–3089.

Schütte, F., Brandt, P., and Karstensen, J., 2016a. Occurrence and characteristics of mesoscale eddies in the tropical northeastern Atlantic Ocean. *Ocean Sci*., 12, 663–685.

Schütte, F., Karstensen, J., Krahmann, G., Hauss, H., Fiedler, B., Brandt, P., et al., 2016b. Characterization of "dead-zone" eddies in the eastern tropical North Atlantic. *Biogeosciences*, 13, 5865–5881.

Sloyan, B. M., Wanninkhof, R., Kramp, M., Johnson, G. C., Talley, L. D., Tanhua, T., McDonagh, E., Cusack, C., O'Rourke, E., McGovern, E., Katsumata, K., Diggs, S., Hummon, J., Ishii, M., Azetsu-Scott, K., Boss, E., Ansorge, I., Perez, F. F., Mercier, H., … Campos, E., 2019. The Global Ocean Ship-Based Hydrographic Investigations Program (GO-SHIP): A Platform for Integrated Multidisciplinary Ocean Science. *Frontiers in Marine Science*, *6*: 445.

Sokal, R. R. & Rohlf, F. J., 1969. Biometry. the principles and practices of statistics in biological research, 2nd edn. San Francisco, CA: W.H. Freeman.

Sutton, A. J. and Sabine, C. L. and Maenner-Jones, S. and Lawrence-Slavas, N. and Meinig, C. and Feely, R. A. and Mathis, J. T. and Musielewicz, S. and Bott, R. and McLain, P. D. and Fought, H. J. and Kozyr, A., 2014. A high-frequency atmospheric and seawater *p*CO_2 data set from 14 open-ocean sites using a moored autonomous system. *Earth System Science Data*, 6 (**2**): 353-366.

Takahashi, T., Sutherland, S. C., Sweeney, C., Poisson, A., Metzl, N., Tilbrook, B., Bates, N., Wanninkhof, R., Feely, R. A., Sabine, C. L., Olafsson, J. & Nojiri, Y., 2002. Global sea–air CO_2 flux based on climatological surface

ocean pCO2, and seasonal biological and temperature effects. *Deep Sea Research Part II: Topical Studies in Oceanography*, 49 (**9-10**), 1601-1622.

Takahashi, T., Olafsson, J., Goddard, J. G., Chipman, D. W., & Sutherland, S. C., 1993. Seasonal variation of CO_2 and nutrients in the high-latitude surface oceans: A comparative study. *Global Biogeochemical Cycles*, 7 (**4**): 843-878.

Tanhua, T., McCurdy, A., Fischer, A., Appeltans, W., Bax, N., Currie, K., et al., 2019. What we have learned from the framework for ocean observing: evolution of the global ocean observing system. *Frontiers in Marine Sciences*, 6: 471.

Tokinaga, H., and Xie, S. P., 2011. Weakening of the equatorial Atlantic cold tongue over the past six decades. *Nat. Geosci*. 4: 222–226.

van Heuven, S., D. Pierrot, J.W.B. Rae, E. Lewis, and D.W.R. Wallace, 2011. MATLAB Program Developed for CO_2 System Calculations. ORNL/CDIAC-105b. Carbon Dioxide Information Analysis Center, Oak Ridge National Laboratory, U.S. Department of Energy, Oak Ridge, Tennessee.

Wanninkhof, R., 2014. Relationship between wind speed and gas exchange over the ocean revisited: Gas exchange and wind speed over the ocean. *Limnology and Oceanography: Methods*, 12 (**69**): 351-362.

Weiss, R., 1974. Carbon dioxide in water and seawater: the solubility of a non-ideal gas. *Marine Chemistry*, 2 (**3**): 203-215.

Whitt, C., Pearlman, J., Polagye, B., Caimi, F., Muller-Karger, F., Copping, A., Spence, H., Madhusudhana, S., Kirkwood, W., Grosjean, L., Fiaz, B. M., Singh, S., Singh, S., Manalang, D., Gupta, A. S., Maguer, A., Buck, J. J. H., Marouchos, A., Atmanand, M. A., … Khalsa, S. J., 2020. Future Vision for Autonomous Ocean Observations. *Frontiers in Marine Science*, 7.

Supplementary Material

Data conversion and flux calculation

According to Wanninkhof (2014), CO_2 fluxes between ocean and atmosphere can be calculated as:

$$FCO_2 = k \times \alpha \times (pCO_2^{SW} - pCO_2^{ATM})$$

where k is the gas transfer velocity for CO_2 (in cm h^{-1}), α is the solubility coefficient of CO_2 (in mol L^{-1} atm^{-1}) calculated as a function of temperature and salinity following Weiss (1974), and pCO_2^{SW} and pCO_2^{ATM} are the seawater and atmospheric partial pressure of CO_2 respectively (in µatm).

The gas transfer velocities have been computed according to the equation proposed by Wanninkhof (2014):

$$k = 0.251 \times U_{10}^2 \times (Sc/660)^{-\frac{1}{2}}$$

where U_{10} is the wind speed (in m s^{-1}), and Sc is the Schmidt number (dimensionless) calculated according to the equation in Wanninkhof (2014). In this study, wind speed measurements acquired by the Saildrone 5 meters above the sea surface level have been used.

Saildrone CO_2 sensor provides the atmospheric and oceanic molar fractions of CO_2 in dry air (xCO_2) which then have been converted into partial pressure of CO_2 (pCO_2) according to:

$$pCO_2^{ATM} = [P_T - (RH/100) \times PH_2O] \times xCO_2^{ATM}$$

and

$$pCO_2^{SW} = (P_T - PH_2O) \times xCO_2^{SW}$$

where PH_2O is the water vapour pressure at the sea surface temperature (in atm) for xCO_2^{SW} conversion and at the atmospheric temperature for xCO_2^{ATM} (in atm) calculated following Dickson et al. (2007), RH is the relative humidity (in %) and P_T is the total atmospheric pressure (in atm) measured by the Saildrone meteorological sensor.

The air-sea CO_2 fluxes were estimated at the same time as the pCO_2^{SW} estimation. Nonetheless, because Saildrone delayed mode data have been binned into different grids (oceanic surface measurements have been binned in 1Hz while data recorded by the CO_2 system are in 2Hz mode and atmospheric data in 20Hz mode), the air-sea CO_2 fluxes were estimated for each xCO_2 measurements, and the closest ancillary data measurements have been used (mean latitude difference = -1.6410×10^{-4}, mean longitude difference = 6.6204×10^{-5}).

Statistical tests

Relationships between xCO_2^{SW}, xCO_2^N and sea surface salinity were computed using a linear regression model. Linear regression statistics, including the standard error of the slope (*i.e.,* the error of the estimated trend), the coefficient of determination (R^2) and the significance of the trend (p-value) were calculated using the

Matlab software. Linear relationships have been tested using the Pearson coefficient for parametric test (Sokal and Rohlf, 1969) with a significance level of 95%.

Deciphering of thermally and non-thermally driven xCO_2^{SW} changes

Thermal (xCO_2^{TD}) and non-thermal (xCO_2^{N}) related effects on the seawater xCO_2 have been calculated in this report according to the following equations proposed by Takahashi et al. (2002):

$$xCO_2^{N} = xCO_2^{SW} \times \exp(0.0423 (T_{mean} - T_{obs}))$$

$$xCO_2^{TD} = \text{mean}(xCO_2^{SW}) \times \exp(0.0423 (T_{obs} - T_{mean}))$$

where xCO_2^{SW} is the mole fraction of CO_2 (in µmol mol^{-1}) measured during the study period, mean (xCO_2^{SW}) is the mean xCO_2^{SW} over the studied period, T_{mean} is the average seawater temperature (in °C, here T_{mean} is equal to 28.24°C) and T_{obs} is the *in situ* seawater temperature (in °C).